Thin Film Transistor Control Circuitry for MEMS Acoustic Transducers

By

Robin Daugherty

A Thesis Presented in Partial Fulfillment
of the Requirements for the Degree
Master of Science

Approved November 2012 by the
Graduate Supervisory Committee:

David Allee, Co-chair
Junseok Chae, Co-chair
James Aberle
Dragica Vasileska

ARIZONA STATE UNIVERSITY

December 2012

ABSTRACT

This work seeks to develop a practical solution for short range ultrasonic communications and produce an integrated array of acoustic transmitters on a flexible substrate. This is done using flexible thin film transistor (TFT) and micro electromechanical systems (MEMS). The goal is to develop a flexible system capable of communicating in the ultrasonic frequency range at a distance of 10 – 100 meters. This requires a great deal of innovation on the part of the FDC team developing the TFT driving circuitry and the MEMS team adapting the technology for fabrication on a flexible substrate.

The technologies required for this research are independently developed. The TFT development is driven primarily by research into flexible displays. The MEMS development is driving by research in biosensors and micro actuators. This project involves the integration of TFT flexible circuit capabilities with MEMS micro actuators in the novel area of flexible acoustic transmitter arrays. This thesis focuses on the design, testing and analysis of the circuit components required for this project.

DEDICATION

I dedicate this thesis to my family

To my mother and father who gave me life

And to the love of my life, Magaline, and our beautiful son Aden

ACKNOWLEDGMENTS

I would like to acknowledge those people who have helped me along the way. All of the faculty members who have guided me in my education have provided me the tools needed to thrive in the field of engineering research. To Dr. David Allee, who showed support of my interest and enthusiasm in circuit design, I could not be where I am without you. To Dr. Junseok Chae, who broadened my horizons by introducing me to the world of micro electromechanical systems, I thank you for the opportunity you provided me. To Dr. James Aberle, who saw the potential in me to assist in teaching the next generation of electrical engineers, I appreciate the chance to contribute to engineering education.

This work could not be accomplished without the contribution of fellow graduate students. I thank Jennie Appel, Alfonso Dominguez, Korhan Kaftanoglu, Sangpyeong Kim, George Kunnen, Edward Lee, Hao Ren, Hellen Schwerdt, Ran Wang, and Xu Zhang for creating an environment of dedication to learning and understanding in the field of research.

TABLE OF CONTENTS

LIST OF TABLES

Page

LIST OF FIGURES

Page

Page

CHAPTER ONE: HISTORY AND STATE OF THE ART

Introduction:

State of the art electronics and micro-machining technology allows for many innovative applications and opportunities for integration. Technologies initially developed for the silicon semiconductor industry can be adapted for use in alternative applications. Two technologies of interest are thin film transistors (TFTs) and micro electromechanical systems (MEMS). TFT circuits are used in large scale integrated applications, particularly in displays and sensing arrays. MEMS technologies on are largely used as discrete components or in small scale micro system applications.

How can these technologies be integrated in a way that is both innovative and practical? MEMS and TFT research have followed a similar evolutionary path; both have developed through the modification of silicon processing techniques for alternative materials to fill applications which traditional silicon semiconductors cannot fill. Until recently, MEMS and TFT structures have been built primarily on crystalline silicon substrates. This not only facilitates the use of silicon processing techniques, but also allows developers to take advantage of the favorable electronic properties of bulk silicon. Recently, TFT fabrication has shifted away from silicon wafer based processing due to attractive niche applications. One of these trends is to replace the rigid silicon substrate with a flexible substrate. This allows engineers to design and fabricate flexible electronic circuits. Historically MEMS have been produced on rigid substrates

with favorable material properties; most common are crystalline silicon and glass. Modern MEMS research has proven that MEMS can be fabricated on flexible substrates.

This common ground between the TFT and MEMS technology allows for flexible integrated micro electromechanical systems. The current research focus is on flexible communication arrays, but the synergy between flexible TFTs and flexible MEMS allows significant room for innovation in both fields. TFTs have proven increasingly useful in control circuitry, especially for in-pixel applications. MEMS technology can be used to design actuators and sensors, which can be used as transmitters and receivers. This report will focus on the design and implementation of the transmitting end of a communication system.

History – Thin Film Transistors:

The concept of the field effect transistor dates back to the 1930's when Lilienfeld (1934) and Heil (1935) introduced the first concept patents for metal/semiconductor transistors. These initial concepts did not lead to working devices until later, when Shockley began experimenting with germanium thin film field effect devices. Unfortunately, these early thin film devices were abandoned at the time in favor of the development of more fruitful junction field effect transistors (JFETs) and bipolar junction transistors (BJTs). Significant development in thin film transistor research began with the work of P.K. Weimer at RCA Labs in the early 1960s. Weimer developed the first working TFTs made

polycrystalline cadmium sulfide using evaporation based processing techniques [1].

In the 1970s the TFT industry found an ideal niche which made TFTs viable in low-cost commercial applications and allowed for a dramatic increase in TFT research. This so called "killer application" was liquid crystal displays (LCDs). In one of the few industries still dominated by vacuum tube technology following the solid state electronics revolution, specifically cathode ray tube (CRT) displays, flat panel display technology was threatening to take over. LCD technology at the time still faced a major problem; without in-pixel switching it was impossible to develop high resolution displays due to crosstalk between pixels. The industry needed transistors, but silicon CMOS could never be adapted to low cost, large area applications. Thin film transistors offered a solution; because TFTs can be fabricated on a variety of substrates and their characteristics are not dependent on the substrate's electrical properties they could be manufactured at a relatively low cost (compared with silicon CMOS) over large areas. Lechner et al. proposed an active matrix liquid crystal display (AMLCD) in which each pixel contains a TFT for pixel switching. Thus the commercial TFT industry was born.

State of the Art – Thin Film Transistors:

The current state of the art in commercial TFTs is still driven by the display industry; however, TFT research has sought out and found niche applications beyond commercial displays. One popular application for TFTs is

sensing arrays. Compatible sensors can be integrated with TFTs to form a large area sensing array [2][3]. The simplest implementation of a large area sensing array would be to use light sensitive diodes to create a photo-detector array; it can even be made using diode connected TFTs if the semiconductor material used in the TFTs is light sensitive. In addition to building sensing arrays, it is possible to build arrays of transducers which act as actuators. By integrating these technologies, one could build a large area array of sensors and actuators.

Based on the ability to fabricate on a variety of substrates, TFT researchers asked the question: can TFTs be fabricated on flexible substrates? TFTs have been successfully fabricated on flexible stainless steel as well as flexible polymer plastics such as polyethylene naphthalate (PEN). The primary fabrication process used for the circuits described in this document has evolved from amorphous silicon (a-Si) insulated by silicon oxide through zinc oxide (ZnO), zinc indium oxide (ZIO) and other mixed oxides, and finally indium gallium zinc oxide (IGZO). These materials are chosen for their electrical properties, specifically the electron mobility and the stability of the threshold voltage [appendix reference]. While these TFTs are developed primarily for the use in active pixel displays, they also provide a solution for fully integrated flexible digital electronics.

History – Micro Electromechanical Systems:

MEMS technology has evolved primarily from the integrated circuits industry. The fabrication techniques developed from the early 1960s following

the invention of field effect transistors have advanced at a tremendous pace, allowing for rapid innovation in integrated circuit manufacturing. In addition to advancement in silicon integrated circuits, these fabrication techniques allowed for development in other fields; one such field is that of micro electromechanical systems (MEMS). The fabrication of planar integrated circuits introduced techniques such as chemical etching, thin film deposition, and other methods to layer three dimensional structures on the surface of a rigid substrate. These methods allowed for micromechanical structures to be produced using essentially the same equipment (though often different materials) used to produce silicon ICs. MEMS research began producing devices such as cantilevers, membranes, and nozzles using a variety of materials and techniques. Additional, the material properties, such as the piezoresistivity of crystalline silicon and the electro-mechanical properties of piezoelectric materials began to be studied and optimized at this time [4].

One essential advantage of the micro-scale processing and micromachining techniques developed for the IC industry and adapted for the micromechanics industry is that of batch processing. Each wafer can be made to contain hundreds of identical structures, allowing for the development of low cost products which employ highly sophisticated circuits and structures. This is most readily observed in the computing industry, where integrated circuits, microprocessors, and imbedded systems are present in many products ranging from personal computers to digital watches and kitchen appliances. MEMS

technology often provides the critical physical interface by integrating micro-scale sensors and actuators. MEMS devices are present in many commercial products including automobiles, ink jet printers and video projectors.

State of the Art - Micro Electromechanical Systems:

The current state of the art in MEMS involves dynamic development in many industries. MEMS development is expensive and time consuming, requiring models and simulations which are constantly refined to properly match experimental results. Fabrication requires time and often the materials are expensive; additionally, each fabrication batch may require revisions to optimize the process flow. MEMS development is very costly and time intensive; the pursuit of such development requires a vested interest in the technology and the possible applications. As a result, much of the work in commercial MEMS revolves around known working device structures for guaranteed performance.

Reliable device structures are the result of millions of dollars spent in research and development from companies like Texas Instruments, Hewett Packard, Bosch and others. Devices such as accelerometers, pressure sensors, actuators, and gyroscopes have become commonplace in automobiles and consumer electronics because the technology has developed to a point where working device structures can be fabricated consistently. More specialized devices, those that have yet to be developed or those that are still in development, require a different kind of dedication.

New and innovative devices are an entirely different challenge; they are not guaranteed to produce results. Often research into the state of the art is done by universities and other research institutions. These environments often allow for investment directly into the science of MEMS with less emphasis placed on fabrication yield and process optimization. Here researchers are able to explore the possibilities of new technologies in attempts to bring them towards maturity.

When new MEMS devices have been thoroughly explored and their merits well understood, they can then be adopted and adapted for commercial production. Thus there is a certain synergy between the academic and the commercial development of MEMS technology. This allows for innovation in many forms; there are new device structures being explored constantly, additionally the devices which show the most promise are continually refined for efficient mass production in commercial applications. The MEMS field has steadily grown to the point where commercial MEMS devices can be found almost anywhere one would care to look.

Bridging the Gap – Integrating MEMS and TFT technology

How do we combine MEMS technology with TFT circuits to encourage innovation and development in both fields while also addressing a specific set of design challenges and research goals in developing a solution for practical applications?

There are many challenges inherent in the art of integration. Research and development often culminates in the integration of two or more seemingly incompatible technologies to produce results which would otherwise be unthinkable. With all of the advances in modern science and engineering in recent years, many design problems can be answered by combining many parts of a whole. Entire development teams are often dedicated to integrating individual components to develop a coherent system. In the case of new technology, particularly in academic research, the focus can sometimes be too narrow to allow for integration. Fortunately, there are some cases wherein research groups are able to work together and combine technology from different fields.

This is the case when it comes to integrating TFT circuits with MEMS devices. This would be a monumental task regardless of the medium chosen employed. Both TFT and MEMS technologies began their early stages of development using primarily single crystalline silicon as a substrate and in the case of TFTs often using silicon as the active semiconductor material. This project develops methods for integrating both mixed oxide TFTs and surface micro machined micro electromechanical devices (MEMS) on the flexible polymer substrate polyethylene naphthalate (PEN).

Challenges

As with any long term design work, there will be challenges in integrating micro electromechanical systems with thin film transistor technology; the solutions will prove particularly elusive due to the flexible medium used for

fabrication. In discussing the potential complications arising in this research, it is appropriate to consider three categories: TFT and Circuit Design, MEMS Design and Mechanical Performance, and Integration. This will allow for the isolation of concerns that are specific to a particular technology or process; many of these problems can be addressed prior to the integration TFTs and MEMS. After isolating specific problems, the focus will shift towards the successful integration of the two technologies; any further complications can then be attributed to the difficulty in integrating these technologies using a medium that is largely experimental.

TFT and Circuit Design Concerns

Structural Stability:

The medium intended for the final realization of this design, poly ethylene naphthalate (PEN), is a flexible polymer material; therefore any other structures fabricated on this medium must also be flexible. TFTs are a natural choice as the semiconductor thin films are naturally somewhat flexible; TFTs are traditionally fabricated on rigid substrates. To address this problem the PEN wafer is adhered to a dummy wafer of silicon or glass so that it will remain rigid during fabrication.

Lithography:

Lithography is already a hot topic amongst the electrical engineering community. As device feature size is scaled down to the micro- and nano-scale the seemingly simply act of *drawing* the features becomes a challenge. Device features must be specified for multiple layers (in industry, mask sets or masks)

and the features must be transferred into physical form, through chemical etching, doping, or film deposition. Lithography techniques must provide sufficient resolution to ensure the successful fabrication.

In the case of fabrication on PEN, the challenge remains. Though the traditional methods of patterning mask sets are applicable in this case, the fabrication engineer must take precaution. Due to the use of a flexible substrate, considerations such as alignment and minimum feature size must be doubly important. TFTs fabricated in PEN cannot be scaled to the extent that state of the art CMOS is scaled (FDC feature size = 10um; state of the art feature size ~ 20nm).

Material Properties:

In many cases, a simplified model is used to describe the operation of a transistor for basic calculations, and more detailed designs are developed using computer aided design tools. With access to these models, the circuit designer rarely needs to consider the electrical properties of the materials used in fabrication. In the case of thin film transistors, the material properties must be modeled as well, but in this case the electrical properties may be affected in unexpected ways. For example in the amorphous silicon process, an outdated process used in previous FDC designs, the electron mobility in the transistors was significantly less than expected. To account for this, measurements have been made and empirical models developed which reflect the device dynamics.

Flexible Circuitry

There are additional challenges stemming directly from the choice of a flexible substrate for the TFT circuits. One of the first concerns is temperature during processing. Commercial CMOS processing involves temperatures exceeding thousands of degrees centigrade. The PEN substrate used in FDC fabrication can only withstand around two hundred degrees centigrade; this means that fabrication engineers must carefully select materials which are compatible with low temperature processing. Additionally due to the flexibility of the substrate many of the techniques used to improve device performance in commercial CMOS are unavailable, such as the technique of using strained silicon to improve the carrier transport efficiency. Essentially, the constraints placed on viable processing techniques create a need for clever innovations in processing as well as in circuit design.

MEMS Design and Mechanical Performance

Structural Stability:

The issue of structural stability affects the MEMS portion of the fabricated system more significantly than it affects the TFTs. This is because of the mechanical nature of the devices. Structures with small moving parts tend to be particularly dependent on mechanical stability for reliable performance. Thus, the challenge is to build a mechanically stable structure on a flexible polymer substrate. The best way to ensure this mechanical stability is to choose the most simple of structures that will achieve the desired effect. The MEMS devices are

simple electrostatic resonators with a suspended diaphragm and a top and bottom electrode; these structures have been shown to allow for a significant level of flexibility while maintaining their structural integrity.

In particular the flexibility of the substrate introduces another effect that is specific to these devices. The performance of electrostatic actuators depends heavily on the diaphragm tension. This means that the mechanical stability of the structure is of particular importance in terms of the frequency and amplitude of the output acoustic wave.

Lithography:

The MEMS fabrication faces the same considerations about lithography, however the device feature size is typically much larger than the TFT counterpart. Instead the alignment of the layers is extremely critical. Proper alignment will result in devices with good stability and thus reliable performance.

Material Properties:

The main consideration in the selection of materials for the MEMS devices is compatibility with the flexible TFT process. Specific considerations include electrical conductivity of the contacts and electrodes, Young's modulus of the diaphragm material, and how the material is typically processed. The method of processing is of particular importance due to the temperature restrictions in processing.

Integration

The preceding discussion has already covered most of the challenges inherent in processing integrated electrical circuitry and electro mechanical devices on flexible substrates. There are a few more considerations that become apparent when attempting to integrate the two technologies together on the same substrate. The biggest issue is compatibility. While past research has discovered semiconductor materials which are compatible with low temperature flexible TFT processing and polymers which are compatible with low temperature flexible MEMS processing, we must consider whether or not these materials are mutually compatible.

The contacts between the TFT circuits and the MEMS device electrodes are of primary concern. While commercial ICs typically use metal layers for routing, the FDC IC process is restricted in temperature. The top "metal" layer used for making contact to the circuits is actually a heavily doped semiconductor material. The MEMS electrodes are metal, either electrodeposited/sputtered aluminum or chrome-gold. These materials are chosen for their adhesion properties when designing the MEMS devices, and compatibility with the FDC IC is largely an afterthought. The result is a large contact resistance due to material mismatch; however, the effect of contact resistance is negligible compared with the effects of leakage in the TFTs and the capacitive load of the MEMS devices.

CHAPTER TWO: SYSTEM OVERVIEW

Introduction

The thin film transistor integrated circuit designed for this project has two primary roles and an additional secondary role. First, the TFT circuit must generate an ultrasonic signal with which to drive the acoustic MEMS; this is achieved using a multi-stage voltage controlled ring oscillator (VCO). Second, the TFT circuit must provide control of the signal flow from the VCO to the MEMS array [2][3][5]. Because this is an experimental circuit, modularity is desired. The TFT circuit design provides options that allow the MEMS devices to be driven by the VCO or by external signals. Additionally, a single signal may be selected as a master signal (one signal drives all channels) or separate signals may be used to drive each channel.

The secondary role of the TFT circuitry is to provide phase control between the channels. With the proper phasing of the driving signal, the output beam of the MEMS array can be steered in directions that are at an angle to the perpendicular direction. Ideally, this control would be fully three-dimensional in the first four octants; this prototype will allow for control only in the lateral plane. This should be sufficient to provide a proof of concept; with further development and more complex control circuitry full control in three dimensions could be achieved.

This section shows the system components, beginning with a system block diagram. Following the system diagram, each circuit will be presented in block

schematic form; the transistor level schematics will be omitted and referenced in the appendices. The core components to be discussed are as follows: ring voltage controlled oscillator (VCO), integrated phase control buffers, MEMS interface output buffers, and integrated control circuitry. The control circuitry will be discussed as part of the system level design.

System Design

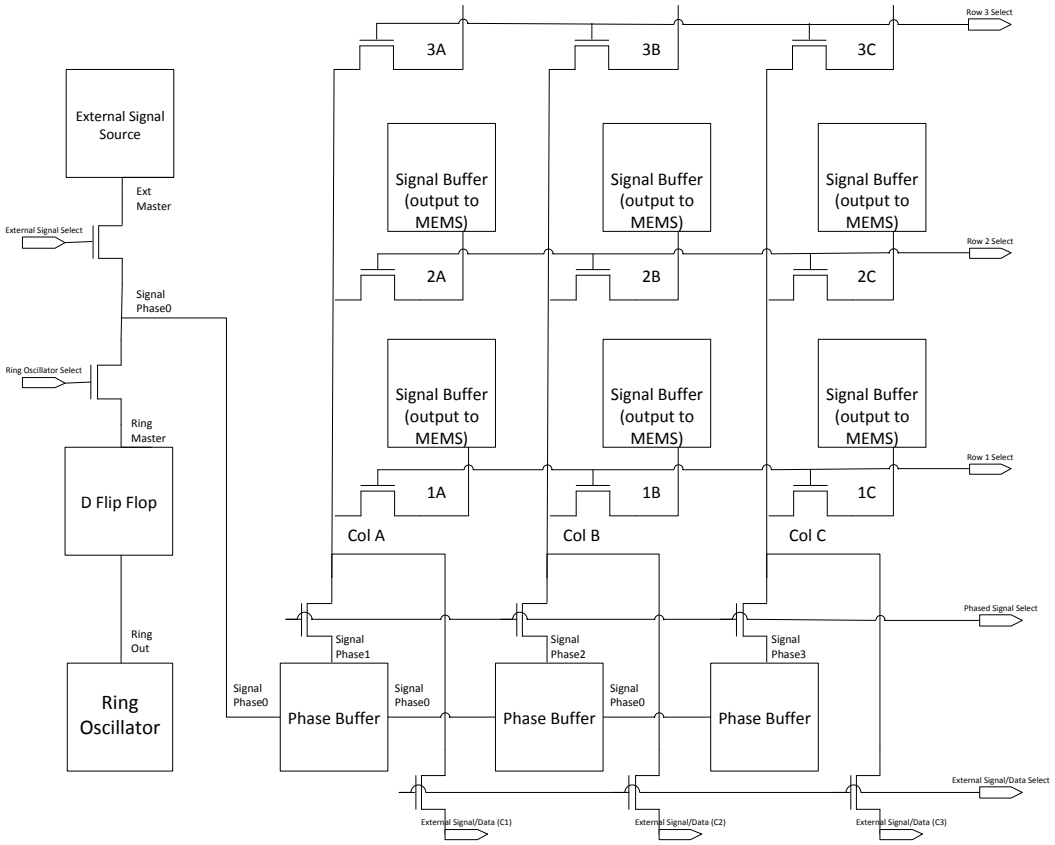

Figure 2-1: System Block Diagram

This gives an accurate representation of the overall system design, including alternative signal sources, control circuitry, phase buffers and output buffers to drive the MEMS devices.

This is the overall system design. The goal of this design is to provide the most flexible prototype solution. To this end, each core component can be effectively bypassed for experimental purposes. While striving for flexibility and functionality as primary goals, the design is also restricted so as to be as simple as possible. Note that there are three channels (columns) across which to phase the

driving signal. This provides for lateral control of the output acoustic wave, while not allowing for full three-dimensional control. Another simplification measure was the choice of a ring VCO as opposed to the preferred LC tank VCO. This allows for the driving signal generation circuit to be purely transistor based; this is most fundamentally compatible with the FDC process.

Ring Voltage Controlled Oscillator

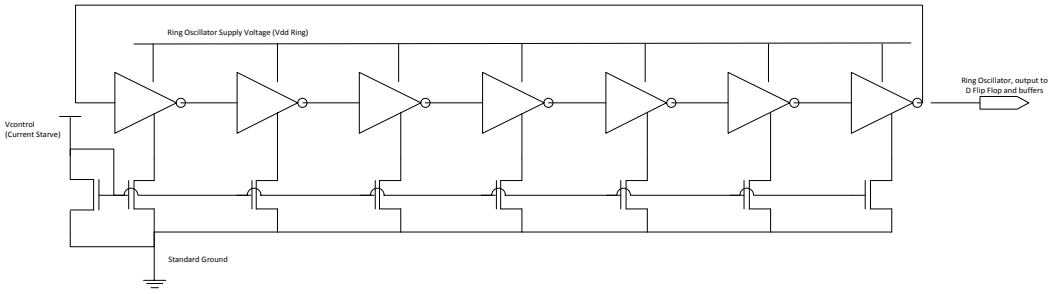

Figure 2-2: VCO Circuit Block Diagram

This gives an accurate representation of the VCO signal generation circuit. The circuit is made up of seven NMOS "bootstrapped" inverters in series. The output is connected in series with the input forming a ring of inverters.

This VCO is the primary signal generating portion of the integrated TFT circuitry. The basic operating principle involves establishing a logical contradiction on each node; by placing an odd number of inverters [6] in a "ring" configuration, the input and output (which are internally shorted) have a contradictory logical value. This fact, coupled with the delay through each stage allows for this circuit to achieve sustained oscillation when provided with DC power. There is technically an alternate state which occurs with an output voltage between the minimum and maximum voltage supply, but this state is unstable,

and a small perturbation (such as that encountered when powering the circuit) will cause the circuit to enter its oscillatory state [7][8].

Each inverter in the ring is coupled to ground through an additional current starving transistor. A current source or even a DC voltage bias at the drain of the current mirror will establish a current through each of the current starving transistors. As the current through the inverters is restricted, the delay for each stage is increased, thus reducing the frequency and allowing for frequency control. Additional frequency control can be achieved by varying the power supplied to the inverters by varying VDD. The principal is the same as that of the current starving, however the output swing will be limited by the supply voltage. This effect is mitigated by the phase control buffers and output buffers, both of which are rail-to-rail buffers.

Phase Control Buffer

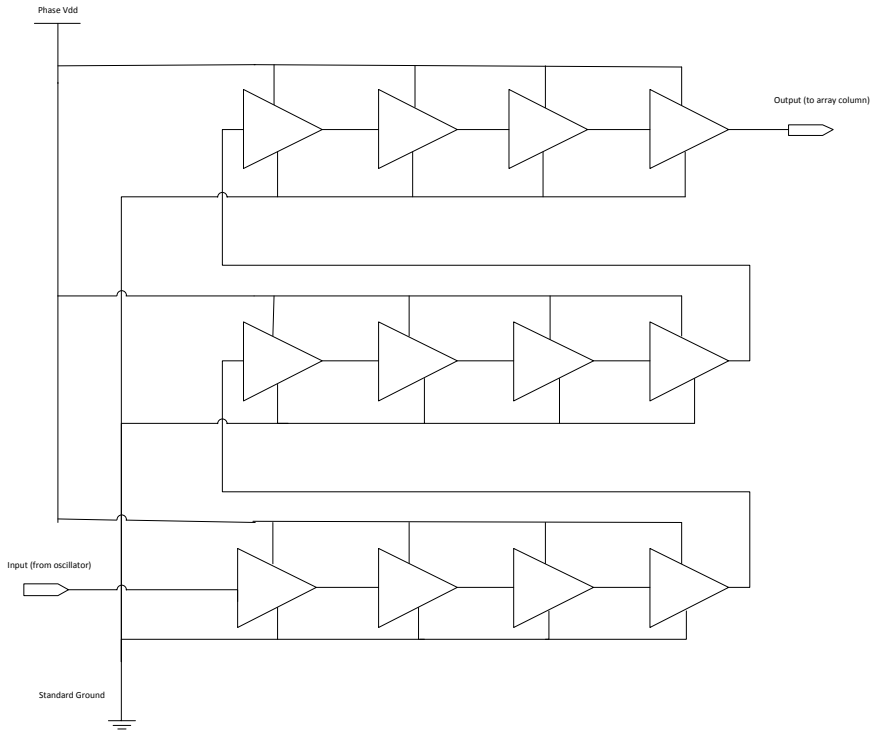

Figure 2-3: Phase Control Buffer Circuit Block Diagram

The phase control buffer is simply a chain of rail-to-rail buffers; each is composed of two inverters in series. The purpose is simply to create a variable delay based on the V_{DD} supplied to the chain.

This is the phase control buffer portion of the design. The operating principle is simple: create a delay in the signal flow by forcing the signal though a series of buffers and control the delay by the applied VDD [9]. The benefit of this circuit is twofold in that it achieves the delay needed to effectively phase the signal applied to each stage, and it also reinforces the rail-to-rail characteristic of the signal if for instance the VCO is supplied with a smaller V_{DD} in order to

reduce the frequency. The phase control is used to steer the beam of the acoustic signal [10][11][12][13].

Output Buffer

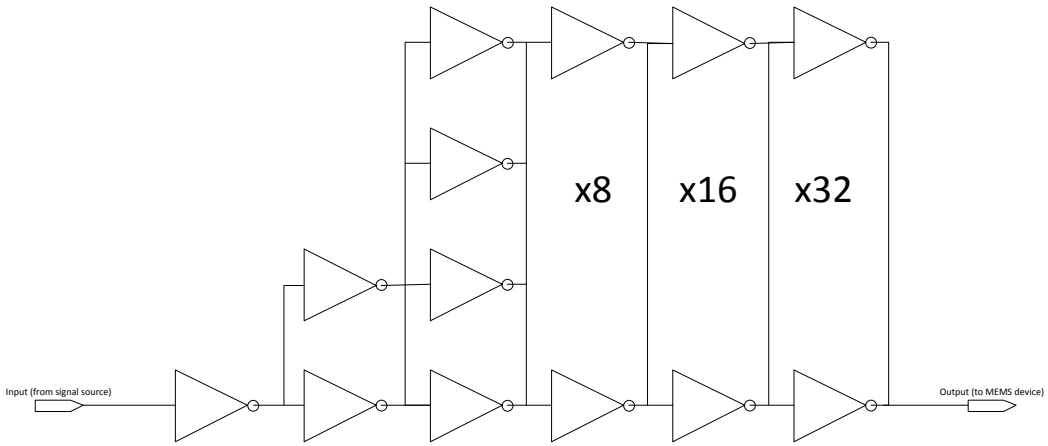

Figure 2-4: Output Buffer Circuit Block Diagram

Similar to the phase control buffer, the output buffer is simply a chain of buffers in series; however in this case the effective size of the buffers is increased by placing several buffers in parallel and increasing this number in each stage between the input and output. This allows the circuit to drive the larger capacitive load of the MEMS devices.

This is the MEMS interface portion of the circuit design. A chain of buffers, increasing in effective size from input to output, make up the output buffer. This allows for the output of this circuit to drive a much larger capacitive load than the VCO output or the phase control buffer output [14][15][16].

CHAPTER THREE: THIN FILM TRANSISTOR CIRCUITS

Introduction

There are several circuits designed specifically for the functional operation of the MEMS ultrasonic array. The primary role of these circuits is to generate the carrier signal, distribute this signal to the array elements, and amplify the signal such that it is sufficient to drive the MEMS actuators. Because the array system is designed to be flexible, much of the backplane circuitry is digital control. This discussion will focus instead on the main functional blocks: a voltage controlled ring oscillator, a phase delay buffer, and a rail-to-rail output buffer. These circuits are all designed and fabricated using a polyethylene naphthalate (PEN) substrate and indium gallium zinc oxide (IGZO) thin film transistors.

Voltage Controlled Ring Oscillator

Operating Principle:

The voltage controlled oscillator is made up of a chain of inverters connected in series; an odd number of inverters are used, and the output is fed back into the input such that neither a high nor a low output is stable. The instability of the output coupled with the delay through each stage causes sustained oscillations which have output swing and frequency dependent on the supply voltage and control.

Procedure:

1) VCO in Isolation
    a. Use probe card to access 2x9 contacts
    b. V_{DD} Ring : [15V, 35V] (higher voltages if necessary)
    c. V_{DD} Ctrl : [15V, 35V] (higher voltages if necessary)
    d. Gnd : 0V
    e. Output : Oscilloscope
2) VCO in Array
    a. Use micro-manipulator probes to access contacts
    b. V_{DD} Ring : [15V, 35V] (higher voltages if necessary)
    c. V_{DD} Ctrl : [15V, 35V] (higher voltages if necessary)
    d. Stnd V_{DD} : [15V, 35V]
    e. Ext Sel 0 : [15V, 35V] = Stnd V_{DD}
    f. VCO Sel : [15V, 35V] = Stnd V_{DD}
    g. Gnd : 0V
    h. Ext In 0 : Oscilloscope

Results:

The VCO has been tested in isolation with a minimal load (parasitic from wiring) and buffered through an additional unity gain buffer to accurately reflect the open circuit voltage output. The results are shown below.

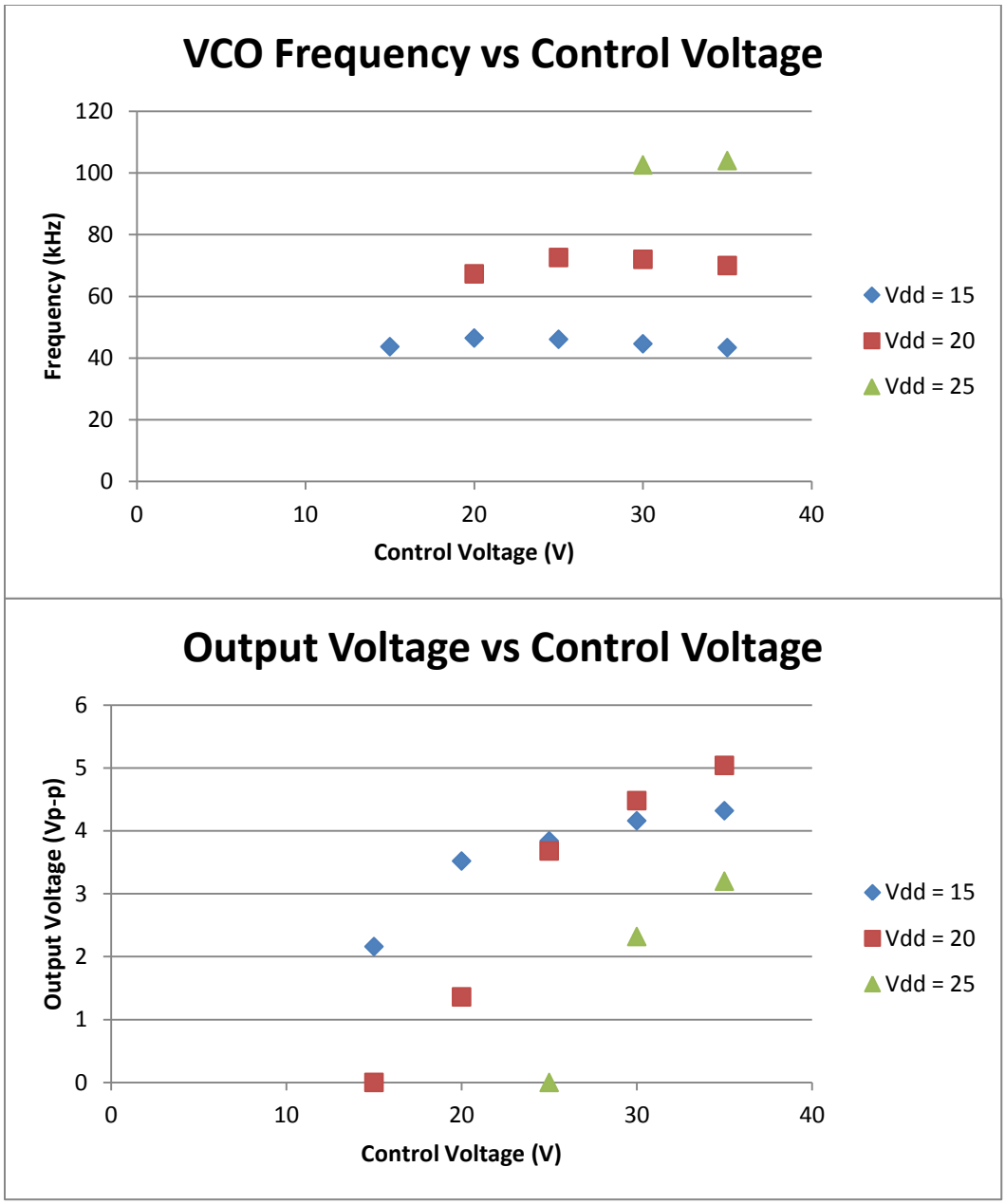

Figure 3-1 (a-b): VCO Frequency and Output Voltage versus Control Voltage

This shows the effect of thee control voltage on the oscillator output. The control voltage has negligible effect on the frequency of the VCO, while it offers nearly linear control of the output voltage.

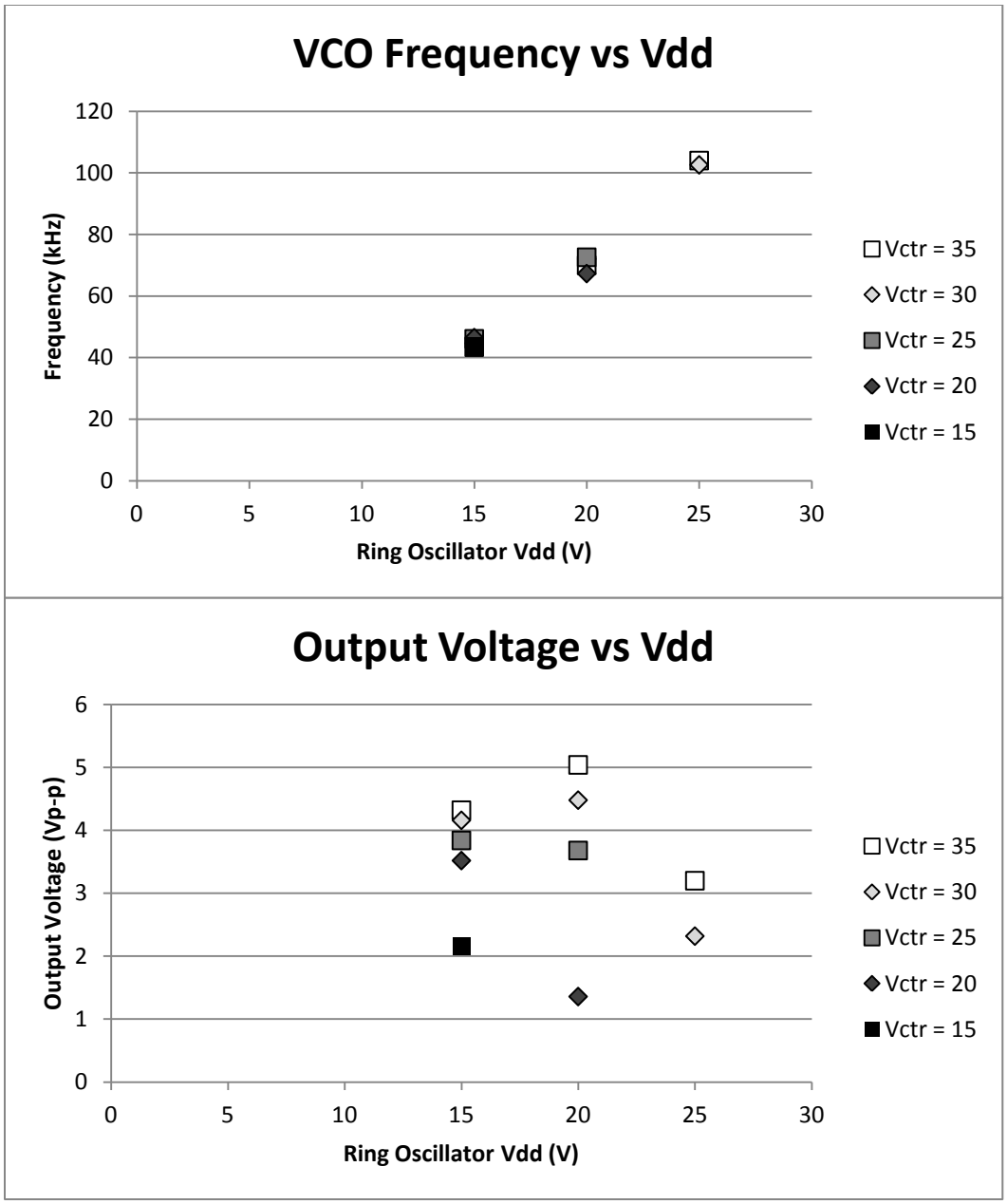

Figure 3-2 (a-b): VCO Frequency and Output Voltage versus Supply Voltage

This shows the effect of thee supply voltage on the oscillator output. The supply voltage offers nearly linear control of the output frequency, but there is very little correlation between the output swing and the supply voltage.

The requirement of the VCO in terms of output is determined differently from the typical case. Normally, the output voltage swing would be considered, because this is the requirement for driving a load. The difference comes from the addition of the rail-to-rail buffering at the output. As long as the VCO provides enough voltage swing to the next stage to cause the first inverter in the buffer chain to switch, the signal will be boosted back towards the rail-to-rail ideal. This is true regardless of the load at the output, so that as long as the oscillator is working properly, the total output voltage swing will be solely a function of the output buffer configuration.

Conclusion:

There are two primary considerations in determining the performance merits of the VCO; first is the frequency, second is the output voltage swing. In fact, the output swing need only be sufficient to drive the next stage so the primary concern is the frequency. The VCO developed for this project has a considerable range of frequency tuning, allowing for full coverage in the low ultrasonic and into the high ultrasonic range. This will allow for the ultrasonic signal to be passed out to the next stage, where it will be buffered in order to drive MEMS transducers.

Phase Delay Buffer

Operating Principle:

The phase buffer is a chain of inverters designed specifically to introduce delay. Under ideal conditions the output will have rail-to-rail swing and be

capable of driving the next stage. The delay is inversely proportional to the supply voltage.

Procedure:

1) Phase Buffer in Isolation
    a. Use probe card to access 2x9 contacts
    b. In : 20 V_{P-P} + 10 V_{DC}
    c. V_{DD} : [15V, 35V] (higher voltages if necessary)
    d. Gnd : 0V
    e. Output : Oscilloscope
2) V CO >> Phase Buffer >> Output Buffer
    a. Use probe card to access 2x9 contacts
    b. V_{DD} Ring : [15V, 35V] (higher voltages if necessary)
    c. V_{DD} Ctrl : [15V, 35V] (higher voltages if necessary)
    d. V_{DD} Phz 1 : [15V, 35V]
    e. V_{DD} Phz 2 : [15V, 35V]
    f. Gnd : 0V
    g. Out 1 : Oscilloscope
    h. Out 2 : Oscilloscope

In isolation, the phase buffer was first tested for the DC behavior. These experiments suggest a complete failure of the circuits, the buffers being incapable of passing either logic high or low. Due to capacitive coupling in the circuits, however, they are capable of passing an AC signal. This feed through path is

extremely lossy, but it may be capable of driving the next stage and the delay through the phase buffer stage can be controlled. This will be the main focus of this report.

An interesting phenomenon has occurred while testing the phase buffers for the MEMS phased array of acoustic transmitters. While there is a sufficiently large phase shift, in lagging and leading phase delays, there is a significant hysteresis phenomenon in the experimental results [17].

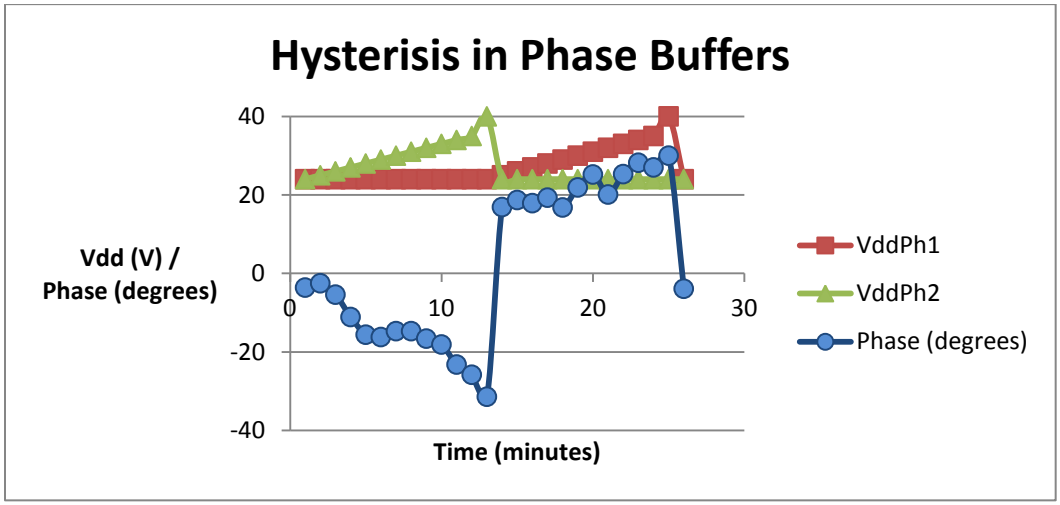

Figure 3-3: Hysteresis in Phase Buffers

Phase shift in buffers shown as a function of time and the applied V_{DD} used to control the phase delay through each buffer.

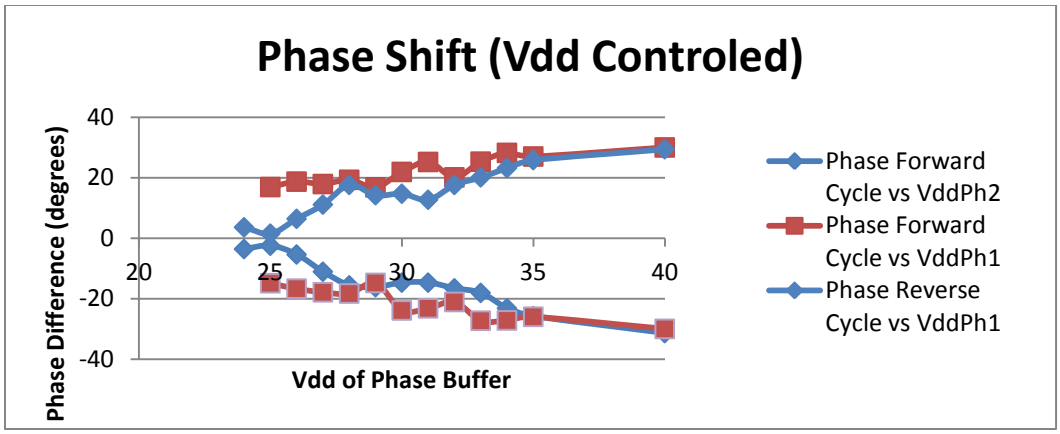

Figure 3-4: Phase Shift versus V_{DD}

Phase shift achieved by varying the V_{DD} of a single phase buffer while holding the other constant. This (Forward Cycle) is the result of first varying V_{DD} of Phase2, then returning to the initial value for both (V_{DD} Ph1 = V_{DD} Ph2 = 24V) and varying V_{DD} of Phase1. A similar result (Reverse Cycle) is attained from first varying the V_{DD} of Phase1 and then varying V_{DD} of Phase2.

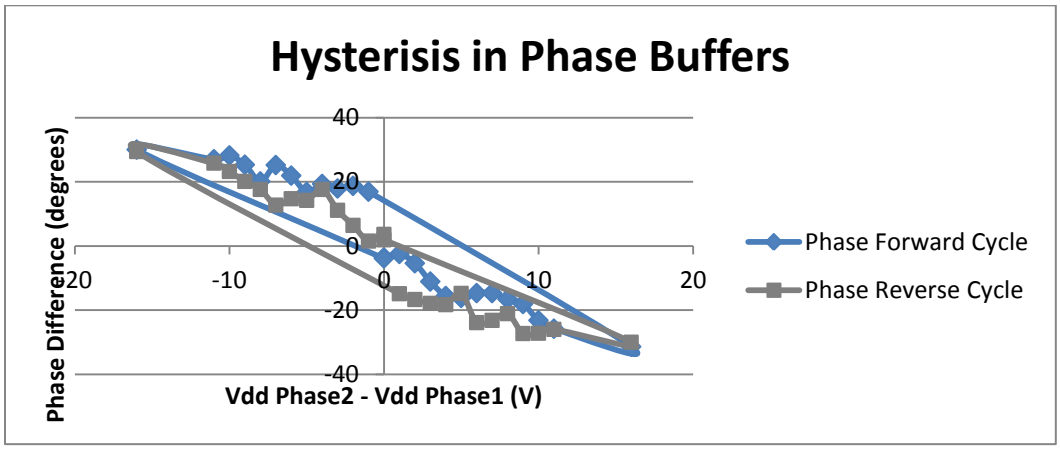

Figure 3-5: Phase difference in the output of the phase buffers

This clearly shows the hysteresis behavior of the phase buffer circuits. The results are generated by first varying V_{DD} of Phase2, then returning to the initial condition, and finally varying V_{DD} of Phase1. A similar result is attained from first varying the V_{DD} of Phase1 and then varying V_{DD} of Phase2.

The hysteresis in the phase buffers has not been exhaustively substantiated; however, it is expected that the hysteresis in the delay through the buffers is due to an underlying hysteresis in the TFT metal-oxide-semiconductor (MOS) capacitance. The MOS capacitance is an intrinsic capacitance formed where the conductive gate material overlaps the transistor channel material. This is typically treated as a parasitic capacitance that increases the RC constant of the transistor; in the case of the phase buffers this leads to a phase delay. The most likely reason for the hysteresis in the gate capacitance is the presence of mobile ion charge (Na^+, K^+). When the circuit is under large bias and high temperature (possibly generated due to carrier self heating effects in the current channel) the ions will shift in position and can cause a change in capacitance [18][19].

Conclusions:

It is readily apparent that there is some level of hysteresis in the phasing buffer operation. This is most likely due to threshold voltage drift, which may or may not be reversible. Since the phase difference will return to its initial condition after a full cycle, it is possible that the threshold voltage has returned to its original value. An alternative explanation would be that the threshold voltages for both phasing buffers have drifted to the tune of an equivalent amount. In this case, repeatable results may not be attainable.

Rail-to-rail Output Buffer

Operating Principle:

The output buffer is a chain of inverters (even number) with increasing fan-out such that a square pulse input will be reinforced at the output. Under ideal conditions the output will have rail-to-rail swing and be capable of driving an RC load. The RC load is low pass filter, attenuating the higher frequency harmonics.

Procedure:

1) Output Buffer in Isolation
    a. Use probe card to access 2x9 contacts
    b. Input : 20 V_{P-P} + 10 V_{DC}
    c. V_{DD} : [15V, 35V]
    d. Gnd : 0V
    e. Output : Oscilloscope
2) Output Buffer in Array
    a. Use micro-manipulator probes to access contacts
    b. Ext In 1 : 20 V_{P-P} + 10 V_{DC}
    c. Stnd V_{DD} : [15V, 35V]
    d. Ext Sel 1 : [15V, 35V] = Stnd V_{DD}
    e. Row 1 : [15V, 35V] = Stnd V_{DD}
    f. Gnd : 0V
    g. Row1/Col1 : Oscilloscope

Results:

The output buffer was first tested in isolation with a minimal load (parasitic from wiring) and buffered through an additional unity gain buffer to accurately reflect the open circuit voltage output. The results are shown below.

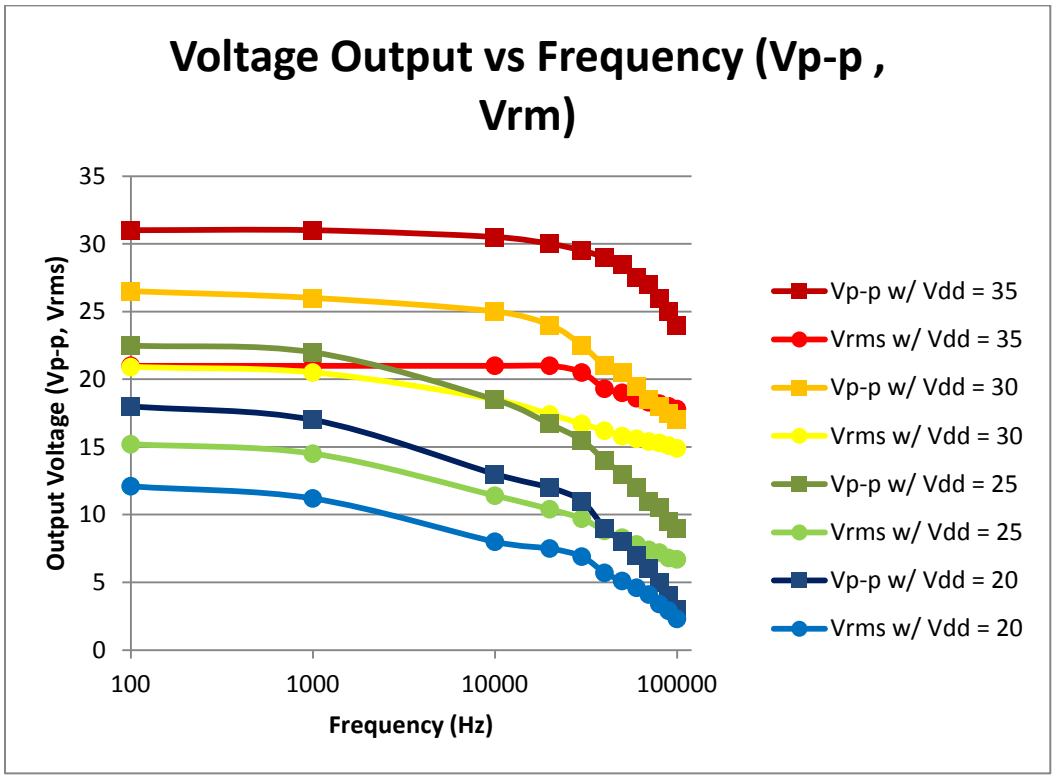

Figure 3-6: Output Voltage versus Frequency of Output Buffer

This shows both the peak-to-peak voltage output and the RMS voltage output. The input signal is a $20V_{P\text{-}P}$ square pulse with a $10V_{DC}$ offset.

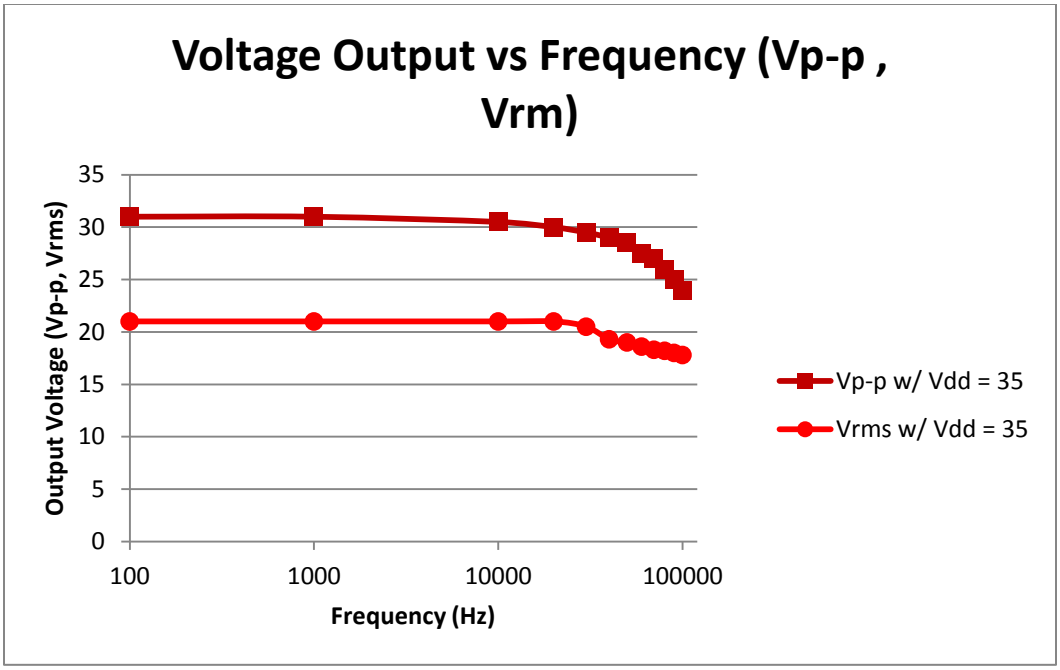

Figure 3-7: Output Voltage versus Frequency of Output Buffer (V_{DD} = 35V)

The largest V_{DD} applied for which the circuits remain stable is 35V; this is typical of the TFTs used in this design. During array operation, this supply level should be the default for the largest driving capability. This will be the focus of the following analysis.

The output swing is attenuated at high frequency due to the parasitic capacitance at the output of the buffer circuits. This allows for almost full rail-to-rail swing near DC conditions, and diminishing output at higher ultrasonic frequencies. The MEMS actuators are most efficient at higher frequencies, so the frequency should be selected for an optimum SPL output by comparing MEMS performance with output buffer performance.

However, in order to correctly optimize for frequency based on TFT/MEMS performance, the TFTs must be tested under loading conditions comparable to that of the MEMS transducers. The results are shown below.

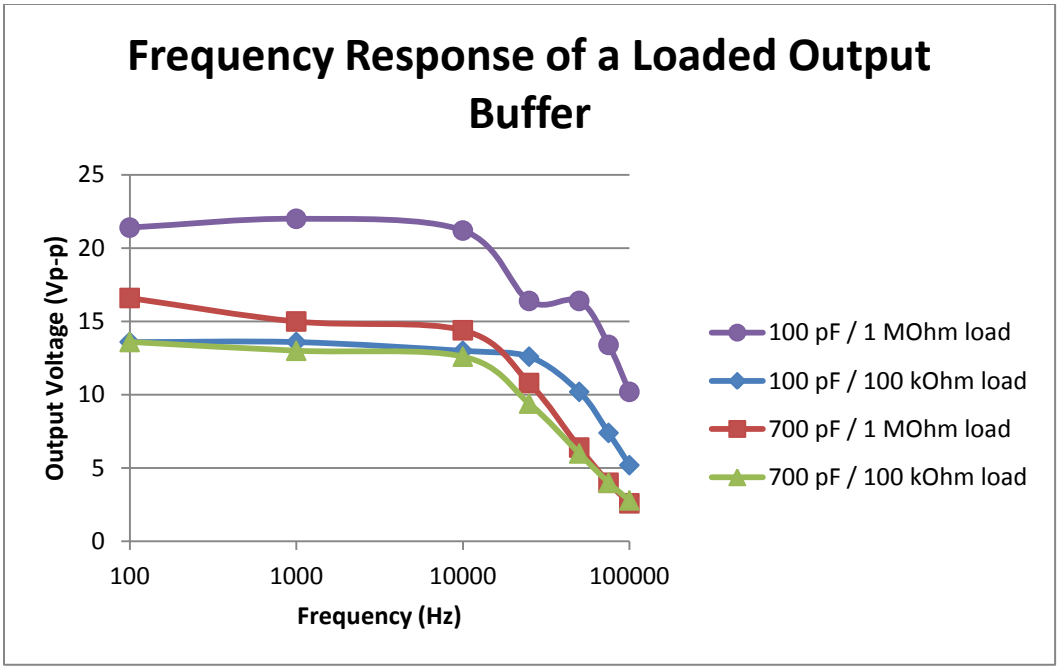

Figure 3-8: Output Voltage versus Frequency of Output Buffer with Passive Load

This shows specifically the peak-to-peak voltage, as this is the critical performance metric which affects the SPL output of electrostatic transducers. The output is connected with an RC load and buffered through a unity gain buffer.

The loads selected for testing reflect the corner cases from empirical C_P-R_P data recorded from the MEMS transducers with capacitive load varying from 100 pF to 700 pF and resistive leakage varying from 100 kilo ohms to 1 Mega ohms. The best case is that which has the smallest capacitance and the largest parallel resistance. The worst case is that which has the largest capacitance and the smallest resistive leakage. The other corner cases show the effect of resistive versus capacitive load; as the resistive path is decreased the DC voltage swing

suffers and as the capacitive load is increased the high frequency performance suffers.

Conclusions:

The load of the MEMS transducer significantly alters the performance of the TFT driving buffers. This must be taken into account for the integrated TFT/MEMS system. The output swing suffers from several pitfalls; there is significant attenuation at high frequency, increasing capacitive load further hinders the high frequency performance, and leakage due to parallel resistance decreases the swing at DC. With the appropriate voltage supply and input frequency, however, the devices should be capable of driving the MEMS actuators with significant SPL output.

CHAPTER FOUR: COUPLED TESTING TFT AND MEMS

Introduction

The development of working MEMS transducers described has preceded the development of the driving circuitry. The reasoning behind this is that an appropriate electrical model for the MEMS must be developed in order to tailor the driving circuitry accordingly. The characterization of the MEMS transducers in isolation has been presented by S. Kim et. al. in [pending publication]. The model can be simplified for electrical analysis and simulation as an RC network with equivalent resistance and capacitance in parallel. The driving circuitry must be robust enough to drive a capacitive load, while the effective output resistance must be kept sufficiently low such that the driving AC signal dissipates power primarily across the load, thus actuating the MEMS transducer and producing an acoustic wave.

The electrical model of the MEMS as driven by an electrical signal source is shown in figure 4-1 [20]; the TFT source consists of a voltage controlled oscillator (VCO), a frequency divider, and an output buffer, but for a simplified analysis the signal source need only be considered as an ideal alternating source with a series resistance and shunt capacitance. This serves as a good model for estimating the frequency response of the transducer load. The full TFT circuit is depicted in block diagram from in figure 4-2 [6][8].

In order to have the greatest advantage of understanding the MEMS/circuit interface, the MEMS were tested with driving ICs as soon as possible. Thus, the

very first generations of working MEMS devices were tested using prototype ICs which were fabricated on silicon using amorphous silicon TFTs. This allowed for the coupling characteristics of the MEMS with IC drivers to be understood and this helped to refine the design process of the final IC design.

The results discussed in this chapter are those found using the second generation of MEMS transducers, and an early prototype of the driving circuitry on silicon. The reason the second generation of MEMS transducers was chosen is because the first generation suffered from a very high failure rate due to difficulties in fabrication (discussed in appendix A) which have since been overcome. Needless to say these results, while encouraging, are suggestive of some necessary design improvements which must be implemented in order to improve the effectiveness of the integrated MEMS on IC solution.

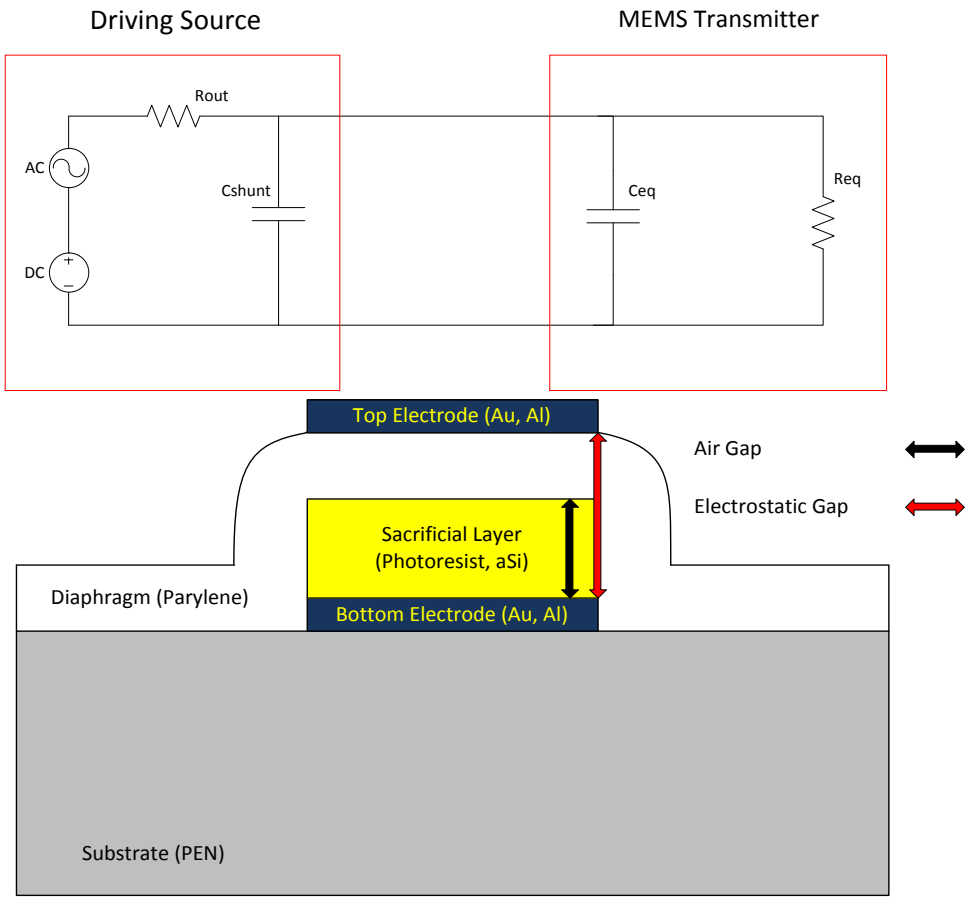

Figure 4-1: MEMS Transducer Equivalent Circuit and Simplified Schematic

(Top) Simplified model of the TFT driving circuit coupled to the MEMS transducer. This is used to estimate the driving capabilities of the TFT driver required to actuate the MEMS and is used primarily for the purpose of simulation. Specifically, if can be used to estimate the frequency response of the loaded driver and determine the electrical power coupled to the acoustic MEMS. Based on physical models of the MEMS transducers, the estimated electrical power coupling corresponds with an acoustic sound pressure level at a given distance from the diaphragm. (Bottom) A simplified schematic view of the electrostatic MEMS transducer is also shown.

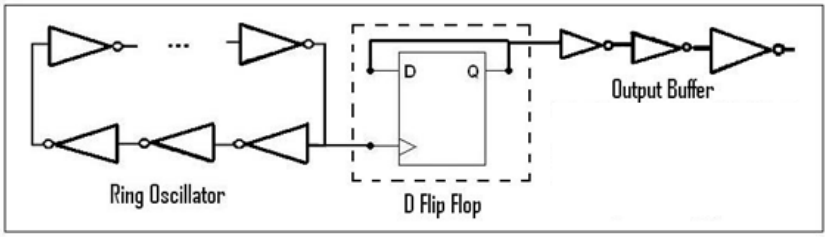

Figure 4-2: System Block Diagram of the TFT Driving Circuit

The ring oscillator (VCO) is used to generate an ultrasonic signal, which may be used to transmit via the MEMS transducers. The output of the VCO itself is not robust enough to drive the device's heavy capacitive load; additionally the leakage resistance of the MEMS transducers requires that the output resistance of the driver be sufficiently low such that a significant portion of the driving power is dissipated across the load. To achieve this, this circuit introduces low output impedance, self biasing output buffer which is capable of sustaining the electrical signal required to produce the necessary acoustic pressure at the output.

Acoustic Testing

The experimental apparatus to test the MEMS transducers coupled with the TFT circuit is quite simple. A condenser microphone capable of detecting high audible to low ultrasonic frequencies (10 kHz – 100 kHz) is used to detect the ultrasonic pressure wave produced by the device. The output can be measured using a spectrum analyzer which is then calibrated to show the received sound pressure level (SPL), a common measure in acoustics of sound intensity [21][21]. In order to determine the range of operation, a rail guided test apparatus is used to mount both the device under test (DUT) and the microphone so that the distance and angle may be precisely controlled. The basic test set up schematic is shown in figure 4-3 and a 3-D model of the rail guided test apparatus is shown in figure 4-4.

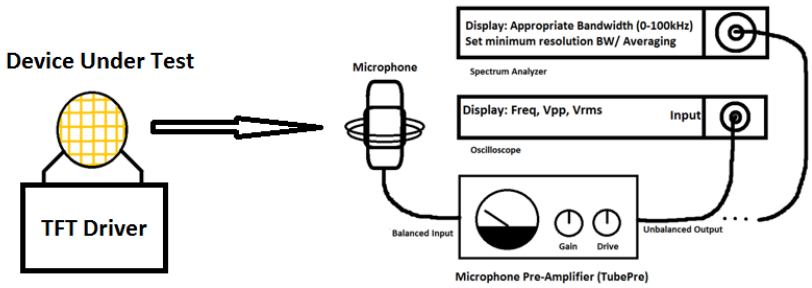

Figure 4-3: Schematic of Acoustic Testing Setup

This is a test system for measuring the acoustic output of the MEMS coupled with TFT driver. The oscilloscope is used primarily as a verification tool while the spectrum analyzer gives an accurate measure of electrical power output from the microphone amplifier, which corresponds directly with the acoustic sound pressure level.

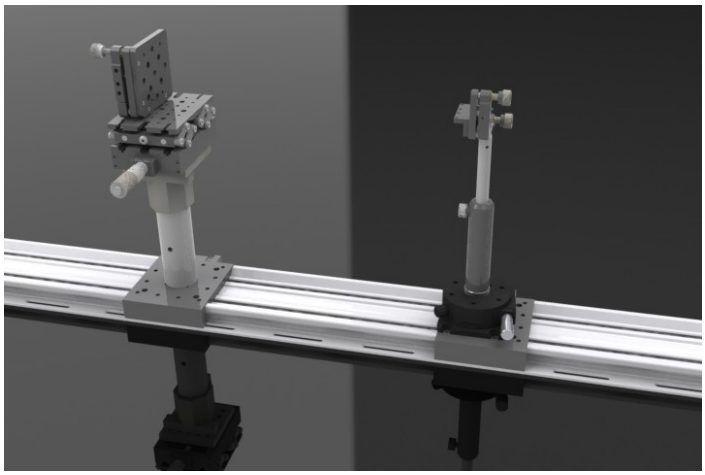

Figure 4-4: Acoustic Alignment System

This is a rail guided system for precisely controlling the distance from the DUT to the microphone and the angle of displacement. Both stands can be moved horizontally along the track as well as vertically and both can be rotated about their center. The stand which holds the DUT can be precisely adjusted vertically for alignment and the stand which holds the microphone can be adjusted radically to within one tenth of a degree.

Results

In presenting the results of the acoustic testing, it is helpful first to demonstrate some justification for the design of the TFT driver. By modeling the output of the driving circuit as an ideal ac voltage source and DC offset with a series output resistance and shunt capacitance and modeling the MEMS transducer as an equivalent resistance and capacitance in parallel we are able to derive the AC response of the coupled driver and MEMS.

By coupling directly to the VCO, the output resistance is fairly large with approximately 150 kOhm. This leads to a large voltage divider when coupled with any leakage path presented by the MEMS transducer. The output buffer significantly reduces this series resistance to a mere 5 kOhm. The simulated AC response of the coupled system is shown if figure 4-5. Considering that the MEMS transducers require at 5 volts DC offset and at least 10 volts peak-to-peak AC to produce a significant acoustic signal, it is clear that the output buffer is necessary to enhance the acoustic output of the coupled system.

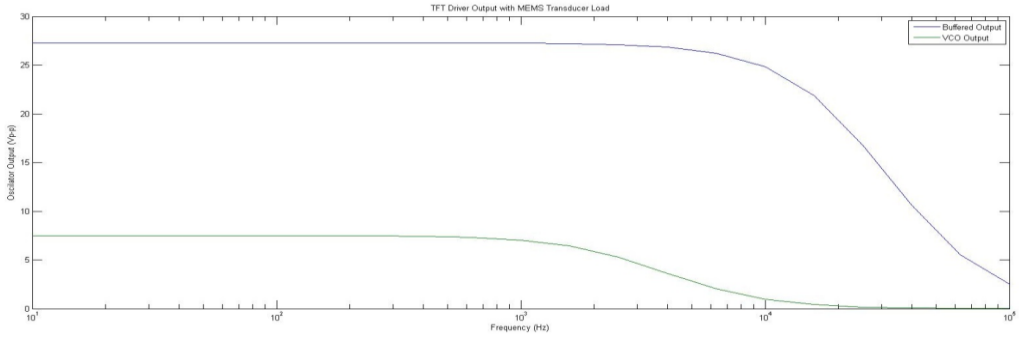

Figure 4-5: Output Voltage versus Frequency of TFT Driving Circuit (Simulation)

Simulated AC response of TFT driver coupled with the MEMS transducer with and without the output buffer. This clearly shows the motivation behind including the output buffer in the system design. The x-axis shows the frequency ranging from 10 Hz – 100 kHz; the y-axis shows the oscillator output swing in V_{P-P}.

The acoustic results are recorded in terms of sound pressure level versus distance. The results are shown in figure 6 along with the theoretical relation based on the near field peak SPL. These results show the sound output for several supply voltages on the TFT driver. The supply voltage affects not only the sound pressure output, but also the frequency. At 30V, 25V and 20V supply voltage, the frequency of actuation is 24.0 kHz, 18.3 kHz and 13.3 kHz respectively.

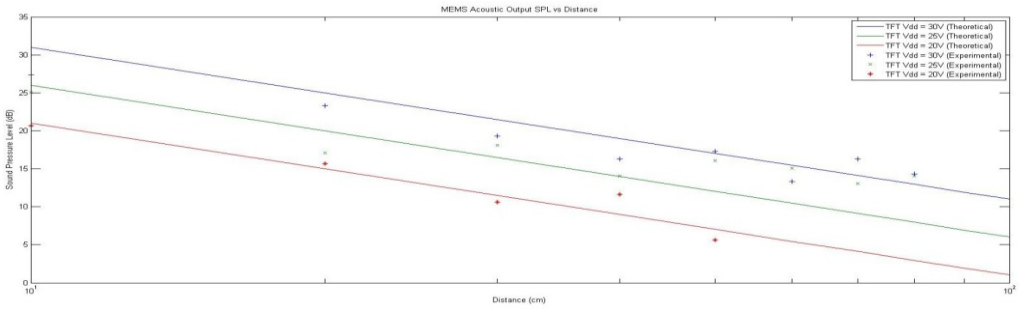

Figure 4-6: Sound Output versus Distance (Theoretical and Experimental)

Results of SPL versus distance of a typical MEMS transducer coupled with amorphous silicon TFT driver. The result shows the expected attenuation of 20 dB-SPL per decade increase in transmission distance. Any deviations in the behavior are likely due to the sharp directionality of the transducer output (making alignment somewhat difficult) or from external factors such as acoustic reflections inside the testing chamber. The x-axis shows the distance ranging from 10 cm – 100 cm; the y-axis shows the sound pressure level measured by the receiver.

CHAPTER FIVE: CONCLUSIONS AND FUTURE WORK

Introduction

The development of an array of MEMS ultrasonic transducers driven by TFT in-pixel circuitry has been completed and tested. The MEMS devices have been shown to work over a limited range of frequency; the frequency range can be controlled by the device structure and can also be tuned using the correct biasing voltage. The TFT circuitry offers a viable solution for array control on a flexible substrate. In this project, the goal was to couple the TFT driving circuitry with the MEMS devices for the purpose of short range communication. The general goal of a coupled MEMS transducer and TFT in-pixel drivers has been achieved; however, there are several difficulties in developing a communications link using this method. The difficulties of this work, along with proposed solutions for future work will be discussed in this section; additionally, alternate applications for this technology will be explored.

Short Range Digital Ultrasonic Communication

One of the primary goals of this research is the assessment of MEMS acoustic transducers as a digital communications link which avoids transmission in the electromagnetic regime. The advantage of this is that the communication link will be immune to electromagnetic interference, which is typically fairly abundant. Where electromagnetic communication often requires narrow-band transmission, ultrasonic communication allows for relatively wide-band transmission. This project attempts to show that such a communications link

using MEMS transducers is possible; however, the capabilities of the prototype system will be somewhat limited.

One of the primary concerns in communications is modulation. Modulation is the way in which digital or analog information is carried by a fundamentally analog signal. The carrier signal can be an electromagnetic signal, such as a radio wave; an electrical signal, in the case of wired transmission; or even in this case, an acoustic signal. Typically, the high frequency carrier signal will be modulated with a lower frequency information signal. At the other end of the link, such as a radio receiver, the carrier signal must be demodulated so that the information signal can be retrieved. Several modulation schemes will be explored and analyzed to determine the best option for acoustic transmission [21]. The best option is typically the option which provides the best signal to noise ratio (SNR).

Modulation Techniques

Amplitude Shift Keying:

Amplitude shift keying (ASK) is a modulation method that uses discrete changes in the amplitude of the carrier signal to convey the information signal. In the case of a digital information signal, only two discrete amplitudes are required. Typically, this modulation scheme can be simplified to use the maximum transmission amplitude and zero amplitude to convey a digital one and digital zero respectively; this is known as on/off keying (OOK). This modulation scheme has the advantage in that it is quite simple to implement. The amplitude

shift keying requires only an amplitude control to modulate the carrier signal; on/off keying requires only an on/off switch to modulate the carrier signal. The disadvantage of this modulation scheme is the signal to noise ratio; compared with other methods of modulation it is quite poor.

Frequency Shift Keying:

Frequency Shift Keying relies on discrete frequencies to convey information. In the case of binary digital information, two frequencies of transmission are required to convey the data. When this is used with a large bandwidth transmission system, the low and high frequency can differ significantly. This is a significant advantage; it means the frequency detector can be fairly imprecise, so long as it is accurate. In order to modulate the carrier signal with this method, the driver must be capable of producing multiple discrete frequencies; this is somewhat more complex than the requirement for ASK, but it is still fairly simple to implement on both the transmitting and receiving end. The advantage of FSK over ASK is improved signal to noise ratio.

Phase Shift Keying:

Phase shift keying (PSK) is a modulation scheme that relies on phase detection at the receiver to demodulate. The information is conveyed by discrete phase shifts in the carrier signal. This modulation scheme requires precise phase control in the transmitter; typically two signals are required: a reference signal and the phase shifted information signal. The advantage of this scheme is significantly better signal to noise ratio, but the hardware requirements are

somewhat extensive. In fact, the hardware requirements are prohibitive in the case of flexible TFT circuits.

The modulation techniques previously discussed are shown below in figure 5-1 and figure 5-2.

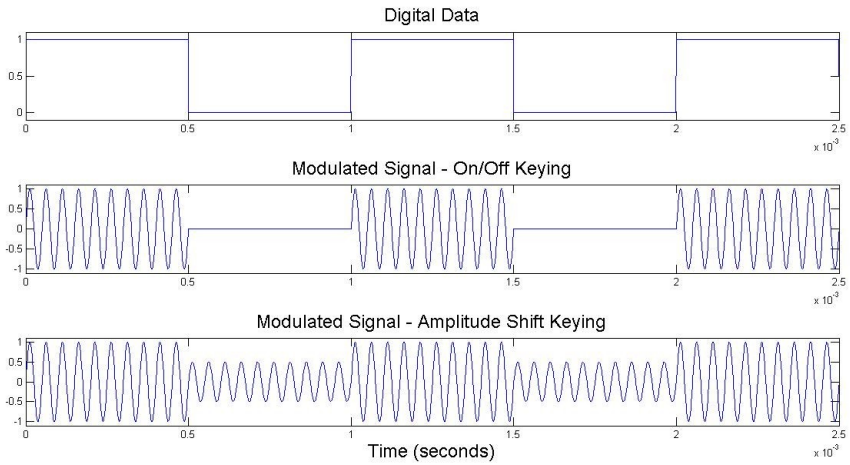

Figure 5-1: Amplitude based digital modulation methods

This plot shows the on/off keying (OOK) and amplitude shift keying (ASK) techniques in their theoretical implementation. The carrier frequency is 20 kHz and the amplitude is arbitrarily set to 1 for the maximum amplitude with 0 and 0.5 for the minimum amplitude of OOK and ASK respectively.

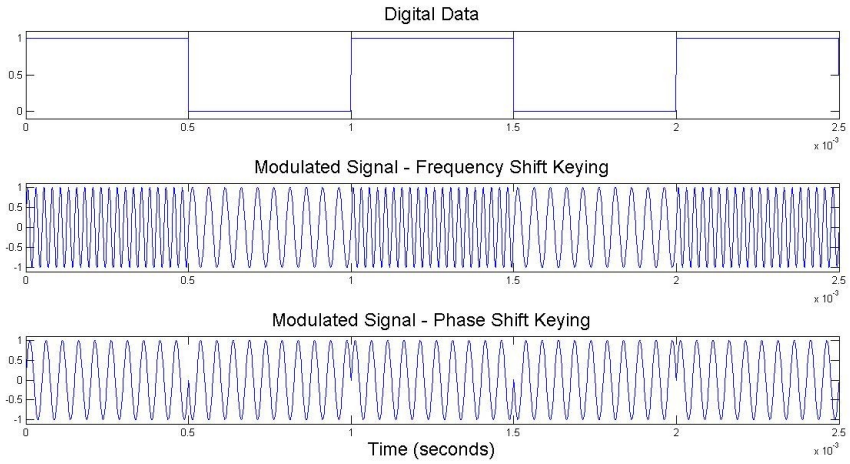

Figure 5-2: Frequency and phase based digital modulation methods

This plot shows the frequency shift keying (FSK) and phase shift keying (PSK) techniques in their theoretical implementation. The amplitude is arbitrarily set to 1 and the carrier frequency is 20 kHz for the PSK and the low frequency of the FSK with 40 kHz for the high frequency of the FSK.

While the modulation selection is fairly important in terms of SNR and complexity of modulation, the MEMS transducers are shown to be capable of any of the three. Frequency, amplitude and phase control circuitry have all been successfully implemented and demonstrated using the TFT circuits chosen to drive the MEMS array. On the other hand, the actual implementation of the modulation scheme was not the focus of this project.

Development of a MEMS ultrasonic data link would require the selection of an appropriate encoding method. It is possible to conceive of a TFT implementation of a frequency shift keying modulation scheme. The driving circuit should include two voltage controlled oscillators, each tuned to the appropriate frequency and a switching circuit which selects between the two VCOs based on the

incoming data. This data could then be modulated over a carrier signal in the ultrasonic range; the carrier signal could be used to actuate the MEMS transducers; and a receiver could be used to demodulate the carrier signal and recover the data. This would be the next logical step to further advance this research.

There are several reasons for selecting frequency shift keying (FSK) as a desirable modulation scheme for a digital transmission system. The core components needed to implement such a system have already been implemented; control circuitry could be developed based on familiar TFT control systems. The amplitude shift keying (ASK) method is only somewhat simpler to implement, but this techniques cannot match the performance of FSK. The phase shift keying (PSK) method offers some advantage, but would require extensive development. The bit error rate (BER) and bandwidth efficiency of each modulation technique are shown below. These simulations highlight some of the advantages of the FSK scheme, in addition to the ease of implementation.

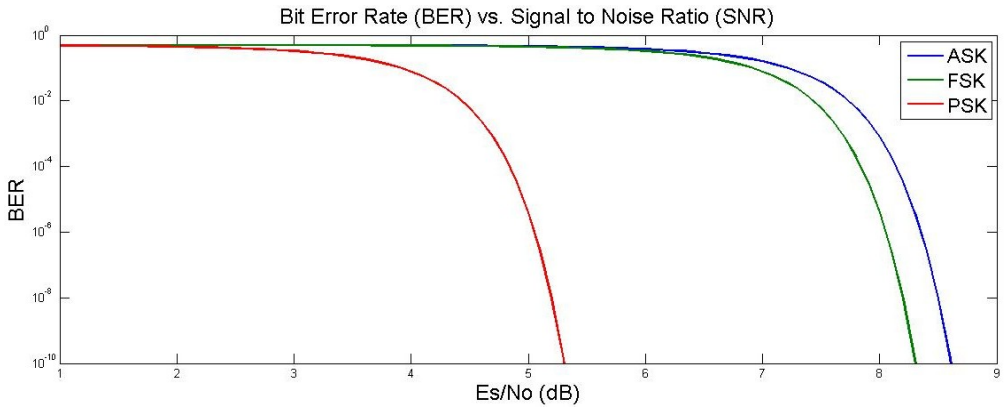

Figure 5-3: Bit error rate of modulation schemes

This plot shows the bit error rate (BER) versus the signal to noise ratio (SNR) defined as the signal power level (Es) over the noise power level (No) expressed in decibels (dB). The PSK method has a clear advantage over the ASK and FSK methods (in the area or 3dB difference for effectively zero errors); however, the FSK method has a slight advantage over the ASK method.

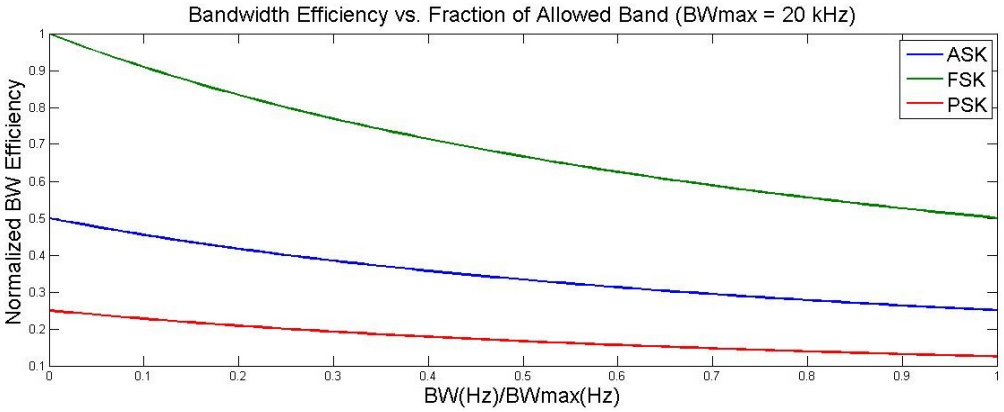

Figure 5-4: Bandwidth efficiency of modulation schemes

This plot shows the bandwidth efficiency versus the fraction of the available band used for transmission. The available band is assumed to be 20 kHz. The FSK modulation scheme a significant advantage in terms of bandwidth efficiency.

Frequency and Phase Sensitivity

This research has introduced circuits which require precise frequency and phase control to be effective. The task of providing a robust method of digital communications using the ultrasonic acoustic range for transmission can only be successful if the transmitted signal adheres to a strict frequency and phase constraints. The experimental results showed promising performance in terms of frequency control; the frequency versus control voltage showed a linear relationship, allowing for accurate control of the frequency. Still, the range of frequency control is process dependent, and all of the circuits tested exhibited degradation over time to some extent.

Additionally, the phase control buffers showed a hysteresis when attempting to adjust the phase delay using the control voltage. This is prohibitive in several possible scenarios. First, this makes it difficult to control the directionality of the phased array. Second, this makes it impossible to implement a phase shift keying (PSK) digital modulation scheme. Both of these scenarios are desirable for an advanced communication system. In order to improve on the functionality of the MEMS ultrasonic array, future research should strive to reduce the effect of hysteresis in the frequency and phase sensitive circuits [22].

Alternative Applications

Limited Distance of Acoustic Transmission:

Another important conclusion of this work is that the transmission range of an acoustic signal is severely limited due to attenuation in air. This means that

the transducer must output at a high volume to reach any reasonable distance. Several Methods have been attempted to increase the transmission distance of a MEMS ultrasonic array. First is to change the size of the diaphragm; however, the correlation between the size of the diaphragm and the sound output are inconclusive. It is clear, rather, that the resonant frequency varies with the size, but this has little effect on the maximum transmission distance. Second is to change the size of the array. In theory, a larger array should output a higher decibel signal which could then be transmitted over larger distances. This will prove to be the case, however the relation between number of array elements and transmission distance is geometric, and therefore the number of elements needed to increase the transmission distance is cost prohibitive.

The results collected during this research project demonstrate the capability of transmitting digital information using an ultrasonic signal across distances exceeding ten meters. This is a considerable achievement considering that the MEMS device structure used in this project is typically used as a sensor. It gives a large electrical response in the presence of a small acoustic pressure; this is ideal for microphones and other sensing applications. Conversely, the MEMS transducer gives a small mechanical response when excited with a large electrical signal. This results in a low decibel sound output which is not ideal for acoustic transmission across a distance. For this reason, it is worth considering these devices and circuits in other applications.

Local Acoustic Transmission:

One alternate application for these MEMS transducers is that of local acoustic transmission. If the MEMS could be tuned to transmit over a wide bandwidth in the audible frequency range, it could replace traditional magnetic speakers. High voltage macro scale electrostatic speakers are commonly used in high fidelity audio systems; these MEMS transducers operate on the same principles. Additionally these MEMS transducers have the advantage of batch fabrication on flexible substrates. Large scale arrays, each containing large number MEMS transducers, could be used as audio frequency loudspeakers.

Because the substrate is flexible these arrays could be used to cover uneven surfaces, such as the interior of an automobile, or the inside of a headset. This is a niche application that could leverage the advantages of this technology. Additionally, the MEMS devices can be made to be incredibly small. This, along with the fact that the MEMS and driving circuitry can be integrated on the same flexible substrate makes these ideal for personal listening devices. Personal listening device applications which could benefit from this technology include hearing aids, Bluetooth telephone receivers, and in ear audio headphones.

In order to approach these applications, the scope of the research would necessarily shift. The primary focus would shift from magnitude of sound pressure output to fidelity of audio reproduction. The use of macro scale electrostatic loudspeakers for high fidelity systems offers evidence that this type of transducer is capable of high fidelity audio. The MEMS devices themselves

must be made to produce an audible range bandwidth with a flat frequency response and minimal distortion. The driving circuit must be designed in a way that minimizes power consumption. They must also be capable of amplifying an electrical signal in the audible frequency range with a flat frequency response, low noise, and minimal distortion [23].

Sensors:

A more plausible alternate application for the MEMS devices fabricated in conjunction with this project is acoustic-to-electrical transduction sensors. In this project the MEMS devices are used as electrical-to-acoustic transducers, with questionable results. Similar devices are typically used as acoustic sensors or pressure sensors. With the right circuitry, these devices could be used in flexible microphone arrays. Large area arrays of microphones are rare, since this would typically require organization of several discrete microphones into array form. These MEMS devices can be fabricated in array form, with the circuitry integrated into the fabrication process.

Microphone arrays have several advantages over a single microphone (or even several microphones not organized in array form). The advantages include fidelity, directionality, source detection and localization. With an array of microphones evenly spaced, the acoustic source can be detected by multiple sensors and the signal can be corrected for phase noise and distortion. In live sound settings, multiple microphones can be used feedback caused by amplification. The increased directionality provided by an array of sensors can be

used to focus on a single sound source, even at a considerable distance. Finally, when properly arranged, the array of microphones can be used for source detection and localization. With the appropriate signal processing algorithms the desired source can be selected based on decibel level relative to a noisy environment, and the acoustic sensing can be localized in that area. This can be used to selectively amplify a single speaker in a crowded conference room [24][25].

Additionally, the size and flexibility of these MEMS devices, along with the ability to integrate control circuitry makes these attractive for applications requiring low form factor microphones. Again, the market for personal listening devices could benefit from this technology. With the right control circuitry, these devices could be used for both microphone and speaker in hearing aids or noise canceling headphones.

In order to approach this application, the scope of the research would again shift. The focus would shift from producing an acoustic signal to detecting an acoustic signal. If the device were used as a simple pressure detector, careful calibration would be required to ensure the accuracy of the detection. If the device were used as a microphone, the fidelity would be a primary concern. The MEMS would need to be designed for a favorable frequency response across the intended range of detection. Also, the circuitry used to amplify the electrical signals produced by the sensing element must preserve the fidelity of the original acoustic signal [23].

Conclusions

This research has shown that MEMS electrostatic transducers can be used to produce an acoustic signal when actuated using a high (~30 V) electrical signal. Prior art in MEMS technology provides strong evidence that these devices can also be used in acoustic sensing applications i.e. microphones. Additionally, this work shows that these MEMS transducers can be integrated with TFT circuitry on a flexible substrate. This fact alone introduces this technology to a field with many possible applications. In this project, the target application was the transmission of digital data using an ultrasonic acoustic signal. The results show that this is possible; digital data can be sent across a short range ultrasonic communications link.

This work serves primarily as a proof of concept that in fact flexible MEMS transducers can be used to transmit data using an acoustic signal. Further work is required to optimize a system that would offer competitive performance. The work required is primarily in the area of signal processing, since the circuits and transducers required to achieve this task have already been developed. However, the MEMS transducers and TFT circuits themselves could benefit greatly from further optimization based on the intended bandwidth and range of transmission.

Other applications have been introduced which could leverage this technology for future research. The fact that these MEMS devices can very likely be used as either sensors or actuators opens up an incredible range of possible

applications. The capability to integrate these sensors and actuators on chip with the driving circuitry is incredibly attractive for integrated applications. The fact that all this can be done on a flexible substrate is not only astounding, it also lends itself well to creative and innovative applications.

REFERENCES

[1] C. R. Kagan and P. Andry, *Thin-Film Transistors*. New York: Marcel Dekker, 2003.

[2] D. M. Raymond, A. J. Lewis, G. Hall and P. H. Sharp, "A prototype pixel readout chip for asynchronous detection applications," *Nuclear Instruments and Methods in Physics Research Section A: Accelerators, Spectrometers, Detectors and Associated Equipment,* vol. 310, pp. 552-556, 12/1, 1991.

[3] M. Raymond, G. Hall, M. Lovell, P. Sharp, C. Lewin and P. Seller, "A 2-D amplifier array chip for pixel detector readout," *Nuclear Instruments and Methods in Physics Research Section A: Accelerators, Spectrometers, Detectors and Associated Equipment,* vol. 348, pp. 673-677, 9/1, 1994.

[4] C. Liu, *Foundations of MEMS*. Upper Saddle River, NJ: Pearson Prentice Hall, 2006.

[5] T. Kishishita, H. Ikeda, T. Sakumura, K. Tamura and T. Takahashi, "Development of a low-noise, two-dimensional amplifier array," *Nuclear Instruments and Methods in Physics Research Section A: Accelerators, Spectrometers, Detectors and Associated Equipment,* vol. 598, pp. 591-597, 1/11, 2009.

[6] Y. Yun, "Bootstrapped inverter using a pentacene thin-film transistor with a poly(methyl methacrylate) gate dielectric," *IET Circuits, Devices & Systems,* vol. 3, pp. 182-186, -08-01, 2009.

[7] M. Soyuer, "A 3-V 4-GHz nMOS voltage-controlled oscillator with integrated resonator," *IEEE J Solid State Circuits,* vol. 31, pp. 2042-2045, -12-01, 1996.

[8] N. Gupta, "Voltage-Controlled Ring Oscillator for Low Phase Noise Application," *International Journal of Computer Applications,* vol. 14, pp. 23-27, -01-12, 2011.

[9] R. J. Bayruns, "Delay analysis of Si NMOS Gbit/s logic circuits," *IEEE J Solid State Circuits,* vol. 19, pp. 755-754, -10-01, 1984.

[10] R. T. Webster and P. H. Carr, "Microwave acoustic and magnetic components for phased array beam steering," *IEEE Trans. Ultrason. Ferroelectr. Freq. Control,* vol. 34, pp. 437-445, 1987.

[11] Y. Je, "Digital beam-steering of parametric array sound beams using piezoelectric micromachined ultrasonic transducers," *J. Acoust. Soc. Am.,* vol. 130, pp. 2464, -10-01, 2011.

[12] E. Yuce and S. Minaei, "A novel phase shifter using two NMOS transistors and passive elements," *Analog Integr. Cir. Signal Proc.,* vol. 62, pp. 77, 01/01, 2010.

[13] S. Minaei and E. Yuce, "High Input Impedance NMOS-based Phase Shifter with Minimum Number of Passive Elements," *Circuits, Systems, and Signal Processing,* vol. 31, pp. 51, 02/01, 2012.

[14] B. A. Rodriguez, "An NMOS buffer amplifier," *IEEE Trans. Electron Devices,* vol. 31, pp. 203-205, -02-01, 1984.

[15] H. Kim, *Array Transducers for High Frequency Ultrasound Imaging,* -01-01, 2010.

[16] J. S. Kim, "Slew-rate-enhanced rail-to-rail buffer amplifier for TFT LCD data drivers," *Electron. Lett.,* vol. 48, pp. 924-U57, -07-19, 2012.

[17] A. Elwakil, "Explaining hysteresis in electronic circuits," *Int J Electr Eng Educ,* vol. 43, pp. 252-260, -07-01, 2006.

[18] D. S. Albin, J. A. d. Cueto, Society of Photo-optical Instrumentation Engineers and National Renewable Energy Laboratory, *Effect of Hysteresis on Measurements of Thin-Film Cell Performance.* Golden, CO: National Renewable Energy Laboratory, 2011.

[19] Huadong Li, G. Subramanyam and S. Dey, "Influence of space-charge on hysteresis loop characteristics of ferroelectric thin films," *Ultrasonics, Ferroelectrics and Frequency Control, IEEE Transactions on,* vol. 55, pp. 286-292, 2008.

[20] B. A. Griffin, M. D. Williams, C. S. Coffman and M. Sheplak, "Aluminum Nitride Ultrasonic Air-Coupled Actuator," *Microelectromechanical Systems, Journal of,* vol. 20, pp. 476-486, 2011.

[21] Chuan Li, D. A. Hutchins and R. J. Green, "Short-range ultrasonic digital communications in air," *Ultrasonics, Ferroelectrics and Frequency Control, IEEE Transactions on,* vol. 55, pp. 908-918, 2008.

[22] C. Li, "Very low hysteresis organic thin-film transistors," *Semiconductor Science and Technology,* vol. 24, pp. 085009; 085009, 2009.

[23] D. Senderowicz and J. H. Huggins, "A low-noise NMOS operational amplifier," *Solid-State Circuits, IEEE Journal of,* vol. 17, pp. 999-1008, 1982.

[24] H. Silverman, "The huge microphone array," *IEEE Concurrency,* vol. 6, pp. 36-36, -10-01, 1998.

[25] B. Rafaely, "The Spherical-Shell Microphone Array," *Audio, Speech, and Language Processing, IEEE Transactions on,* vol. 16, pp. 740-747, 2008.

[26] M. Auphan and H. Dormont, "Pulsed acoustic radiation of plane damped transducers," *Ultrasonics,* vol. 15, pp. 159-168, 7, 1977.

[27] A. Freedman, "Acoustic Field of a Pulsed Circular Piston," *J. Sound Vibrat.,* vol. 170, pp. 495-519, 3/3, 1994.

[28] D. Perov, "Analysis of wavefronts for the piston source acoustic fields," *J. Acoust. Soc. Am.,* vol. 123, pp. 3847, 2008.

[29] P. Hariharan. *Optical Interferometry* 2003.

APPENDIX A
DATA COLLECTED JANUARY 2011 – OCTOBER 2012

APPENDIX A: MEMS ELECTROSTATIC TRANSDUCERS

A1: Electromechanical Models for MEMS Transducers

The primary functional component for the MEM ultrasonic array is the custom flexible MEMS transducers which transmit the acoustic wave into the air. These devices operate on the basic principle of electrostatic acoustics; however, there are several innovations that make them unique. This chapter will discuss the design and operating principle, as well as some of the basic models used to describe the devices and estimate the performance under ideal conditions. First, the device structure will be described, while a detailed description of the fabrication process will be reserved for the appendices. Next, the basic operating principle of electrostatic devices will be discussed, followed be a more detailed discussion of the device specific performance. Finally, we will use this analysis in order to estimate the output sound pressure levels and the range of acoustic transmission [20].

The devices designed for the ultrasonic array described in this project are based on the principles of electrostatic actuation. Specifically, the MEMS transducer is a micro-scale version of an electrostatic loudspeaker. An electrostatic loudspeaker is a speaker which generates sound by a vibrating membrane suspended in an electrostatic field. The membrane must be thin and flexible and it is coated in a conductive material such as graphite; it is suspended between two conductive grids or electrodes. A bias voltage is applied to the electrodes in order to tension the diaphragm for maximum sound output. A large

AC signal is used to actuate the diaphragm. If a uniform electric field is produced by the electrodes, the sound output will have a high signal-to-noise ratio (SNR) and a linear response at high frequencies.

The advantages of electrostatic actuation for audio reproduction are clear. The response of such systems is significantly more predictable than that of typical dynamic speakers. Thus, characterizing these systems offers significantly lesser burden as compared with traditional dynamic systems. However, this project calls for micro-scale sound output devices which operate in the ultrasonic range. Electrostatic MEMS can be used to meet this requirement, and they offer many favorable characteristics. There are also a significant number of challenges which will be addressed in this chapter.

Design decisions will focus on maximizing sound output in the ultrasonic range for maximum distance of acoustic transmission. The operating parameters of these devices must be determined in order to design optimal circuitry to drive an array of ultrasonic MEMS. This chapter will also discuss the experimental performance of the fabricated MEMS. These results are used primarily to justify circuit design decisions made with the intention to optimize the sound output of a 3-by-3 array. This small array of devices will serve as a proof of concept, and large scale arrays would operate on the same principles employed in this paper.

Basic Device Structure and Operating Principles

This section introduces a simplified device structure for the MEMS actuator and an electromechanical model used for theoretical analysis. The true

device structure will differ slightly, due to fabrication techniques and limitations, but this model is sufficient for developing an understanding of the device performance. Figure 6-1 shows the simplified device structure.

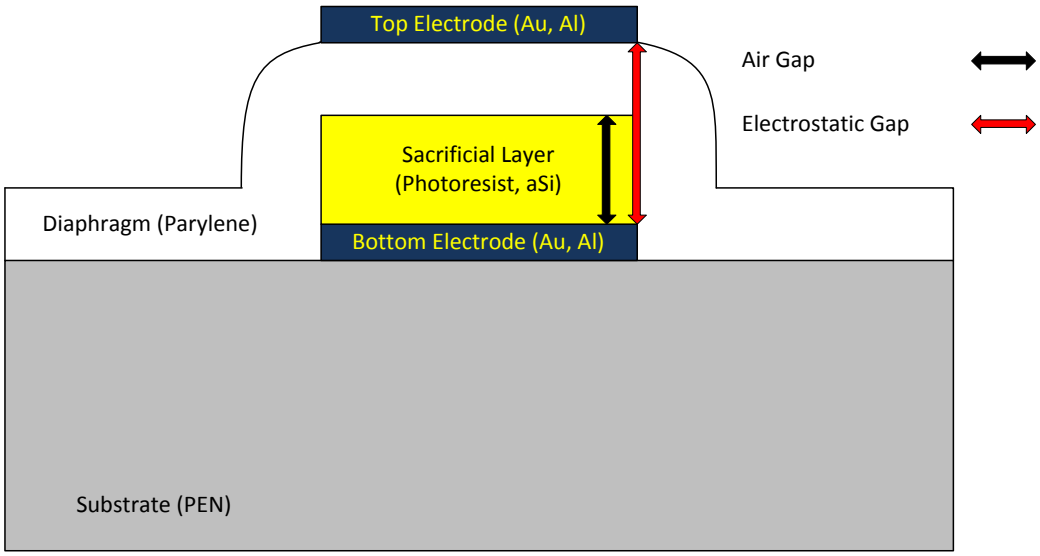

Figure 6-1: MEMS Device Structure Schematic

Simplified device structure shows the substrate (initially silicon is used for proof of concept, eventually silicon is replaced with PEN), the electrodes (gold or aluminum) and the diaphragm. The electrodes provide the electrical force and the diaphragm provides the mechanical forces. These forces in conjunction allow for actuation of the diaphragm.

In order to begin the analysis of this structure, and electromechanical model must be adopted. The model will be quite simplified, as it will only be used to predict the biasing conditions and appropriate actuating amplitude of the applied voltage. The devices will also be electrically tested in order to find the optimal biasing conditions based on the actual device performance. Figure 6-2 shows the simplified electromechanical model.

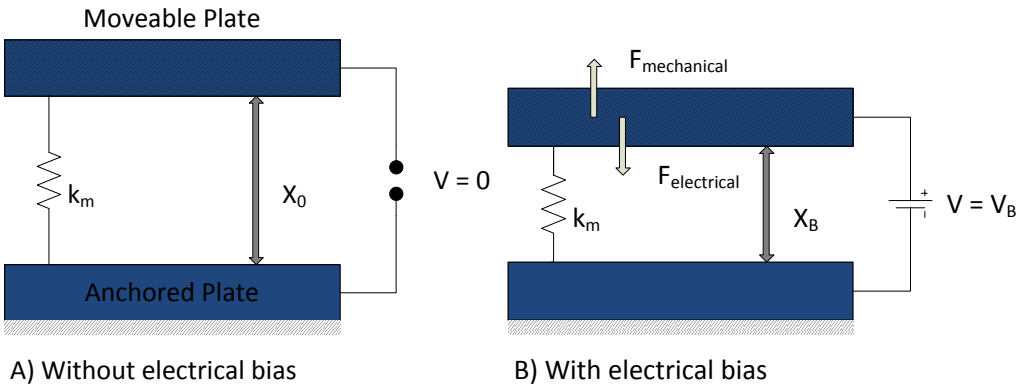

Figure 6-2: MEMS Electro-Static Model

Simplified electro-static model show the electrodes in two configurations: (A) shows the electrodes with no bias applied; the diaphragm is at its normal resting position; (B) shows the electrodes with a voltage bias applied; the electrostatic force pulls the moveable electrode toward the anchored electrode while the mechanical force pushes the moveable electrode up away from the anchored electrode.

Theoretical Analysis is as follows:

Electric force in terms of capacitance (C), voltage (V), and electrode geometry (A, d)

$$F_{electric} = \frac{1}{2}\frac{\varepsilon A}{d^2}V^2 = \frac{1}{2}\frac{CV^2}{d}$$

Electric force in terms of initial spacing (x_0) and displacement (x)

$$F_{electric} = \frac{1}{2}\frac{\varepsilon A}{(x_0 + x)^2}V^2 = \frac{1}{2}\frac{C(x)V^2}{2(x_0 + x)}$$

Mechanical force in terms of spring force constant (k_m) and displacement (x)

$$F_{mechanical} = -k_m x$$

Spring constant of a circular diaphragm in terms of radius (R), thickness (t), Young's modulus (E), Poisson's ratio (ν), and residual stress (σ)

$$k_m = \frac{16\pi E t^3}{3R^2(1-v^2)} + 4\pi\sigma t$$

Pull in voltage is the voltage at which the F(x) curves for electrical and mechanical force versus displacement intersect tangentially. Beyond this voltage, the electrical force will overwhelm the mechanical force and the device will collapse.

Pull in voltage in terms of initial spacing (x_0), spring force constant (k_m), and capacitance (C_0)

$$V_p = \frac{2x_0}{3}\sqrt{\frac{k_m}{1.5C_0}}$$

As it turns out, the maximum efficiency of electromechanical actuation is achieved by operating the device at a bias voltage near to this pull in voltage. The device must be carefully analyzed, and the bias and operating conditions must be chosen carefully.

Device Geometry and Predictions:

All of the MEMS devices created for this project will have micro-scale dimensions. The diaphragm and electrodes will all be circular with diameters on the order of millimeters. The air gap between the diaphragm (moveable electrode) and the substrate (stationary electrode) will be on the order of microns. In the fabrication of suspended diaphragm devices, the minimum air gap is limited mined by the process used to make the structure. In the process used for

this project, a sacrificial layer is deposited on top of the bottom electrode. This sacrificial layer fills the space of the air gap and the diaphragm and top electrode are fabricated atop. When the subsequent layers have been fabricated, the final step in the process is to release the device, that is, to etch away the sacrificial layer leaving only the suspended diaphragm and an air gap between the top and bottom electrodes.

The release of the structure is the critical step in determining the minimum air gap. Two distinct materials have been selected to facilitate this step. The sacrificial layer will be made using either the photo resist AZ9260 or amorphous silicon (a-Si). The AZ9260 sacrificial layer will be etched using a wet etch and the devices must be allowed to dry. This introduces the problem of stiction, a process by which the surface tension of the liquid etchant causes the diaphragm to collapse as the device dries. Stiction effects limit the minimum air gap in AZ9260 devices to 4-6 um. The a-Si sacrificial layer will be etched using a dry plasma etch, which eliminates the effects of stiction. These devices can be produced with an air gap as small as 1-2 um.

Table A1-1: Mechanical properties of circular parylene diaphragms of varying size with 2um amorphous silicon sacrificial layer

Diameter (mm)	Radius (mm)	Thickness (um)	Young's Modulus (Pa)	Poisson's Ratio	Residual Stress (MPa)	Spring Constant
2	1	2	400000	0.4	100	2510
3	1.5	2	400000	0.4	150	3770
4	2	2	400000	0.4	200	5030
5	2.5	2	400000	0.4	250	6280
6	3	2	400000	0.4	300	7540

Table A1-2: Mechanical properties of circular parylene diaphragms of varying size with 4um AZ9260 sacrificial layer

Diameter (mm)	Radius (mm)	Thickness (um)	Young's Modulus (Pa)	Poisson's Ratio	Residual Stress (MPa)	Spring Constant
2	1	2	400000	0.4	100	2510
3	1.5	2	400000	0.4	150	3770
4	2	2	400000	0.4	200	5030
5	2.5	2	400000	0.4	250	6280
6	3	2	400000	0.4	300	7540

Table A1-3: Mechanical properties of circular parylene diaphragms of varying size with 6um AZ9260 sacrificial layer

Diameter (mm)	Radius (mm)	Thickness (um)	Young's Modulus (Pa)	Poisson's Ratio	Residual Stress (MPa)	Spring Constant
2	1	2	400000	0.4	100	2510
3	1.5	2	400000	0.4	150	3770
4	2	2	400000	0.4	200	5030
5	2.5	2	400000	0.4	250	6280
6	3	2	400000	0.4	300	7540

Table A1-4: Pull-in voltage of circular parylene diaphragms of varying size with 2um amorphous silicon sacrificial layer

Diameter (mm)	Radius (mm)	Area (mm^2)	Cap Gap (um)	Spring Constant	Capacitance (pF)	Pull-in Voltage (V)
2	1	3.14	4	2510	0.69	20
3	1.5	7.07	4	3770	1.56	17
4	2	12.6	4	5030	2.78	15
5	2.5	19.6	4	6280	4.34	13
6	3	28.3	4	7540	6.36	12

Table A1-5: Pull-in voltage of circular parylene diaphragms of varying size with 4um AZ9260 sacrificial layer

Diameter (mm)	Radius (mm)	Area (mm^2)	Cap Gap (um)	Spring Constant	Capacitance (pF)	Pull-in Voltage (V)
2	1	3.14	6	2510	0.46	50
3	1.5	7.07	6	3770	1.04	40
4	2	12.6	6	5030	1.85	35
5	2.5	19.6	6	6280	2.90	32
6	3	28.3	6	7540	4.17	30

Table A1-6: Pull-in voltage of circular parylene diaphragms of varying size with 6um AZ9260 sacrificial layer

Diameter (mm)	Radius (mm)	Area (mm^2)	Cap Gap (um)	Spring Constant	Capacitance (pF)	Pull-in Voltage (V)
2	1	3.14	8	2510	0.34	90
3	1.5	7.07	8	3770	0.78	70
4	2	12.6	8	5030	1.39	60
5	2.5	19.6	8	6280	2.17	55
6	3	28.3	8	7540	3.13	50

The pull in voltage varies significantly with device geometry, so the circuit design must allow for various biasing conditions. However, the amplitude relative to the bias voltage should be similar. Thus, it is sensible to design a voltage controlled oscillator which will swing from rail-to-rail with respect to the supply voltage, and the biasing voltage can be chosen as half of the V_{DD} rail voltage.

This will allow for various device geometries to be used in early prototypes. By testing various device geometries, this experiment will determine which is the most efficient in terms of sound output generated for a given input power. From there, the most efficient devices will be chosen for an array of transmitting devices. This ultrasonic array is the overall end goal of this project.

A2: Equivalent Circuit Electrical Model

In designing circuits to interface with MEMS devices, it is useful to have an equivalent circuit model for the MEMS component in order to facilitate circuit simulations. In the case of the thin film TFTs used in this project, very accurate simulations can be performed in HSPICE using BSIM3 equivalent transistor

models. However, HSPICE is not capable of handling mechanical components in simulation, so the MEMS model must be simplified. Equivalent electrical circuit models allow for the simulation of *circuit* performance; the MEMS device performance must be treated separately. Due to the complexity of the physics of mechanical oscillating membranes, the treatment must be verified using experimental results.

Thus, the equivalent circuit models will be developed for use purely in simulating the performance of the interface circuitry, and will not help us to describe or to analyze the performance of the MEMS devices themselves. A simple equivalent circuit is introduced below. The equivalent circuit takes an extremely simplified view of the MEMS component. The capacitance is taken as a simple parallel plate capacitor which has an air gap equal to the initial position of the diaphragm. The assumption that the capacitance is constant is a significant simplification because in reality the capacitance varies as the diaphragm becomes displaced. One acceptable way to compensate for this is to overestimate the equivalent capacitance to be sure the driving transistor fan-out can drive the capacitive load.

The resistance component of the equivalent circuit is more difficult to justify. In one sense, there *is* a physical resistance to diaphragm deflection due in part to the spring restoring force and in part to air resistance. This physical resistance, however, is *not* the reason for the electrical resistance in the equivalent circuit. Due to difficulty in fabricating devices with complete isolation between

the top and bottom electrodes, there is a resistive leakage path. This can be due to several problems encountered during fabrication. When metal layers are deposited on flexible, porous polymers, there is a chance for "stringers" to develop which create resistive current channels between the electrodes. During the sputtering process metal ions may find their way into the air gap between the electrodes; if the diaphragm is not properly suspended (if it is partly collapsed) the ion can behave somewhat like a "trap" level in a semiconductor, creating another path for discharge between the two electrodes. Other second order effects may also come into play. Any resistive leakage paths in the MEMS device can be simplified as an equivalent resistance. In order to ensure the output resistance of the driving circuit is small enough that the AC voltage is dropped primarily across the RC load presented by the MEMS; the equivalent resistance will be taken as the minimum measured resistance of the MEMS devices.

By taking an equivalent circuit model which represents the least efficient load configuration, the driver can be designed to be robust. The equivalent circuit schematic is shown below.

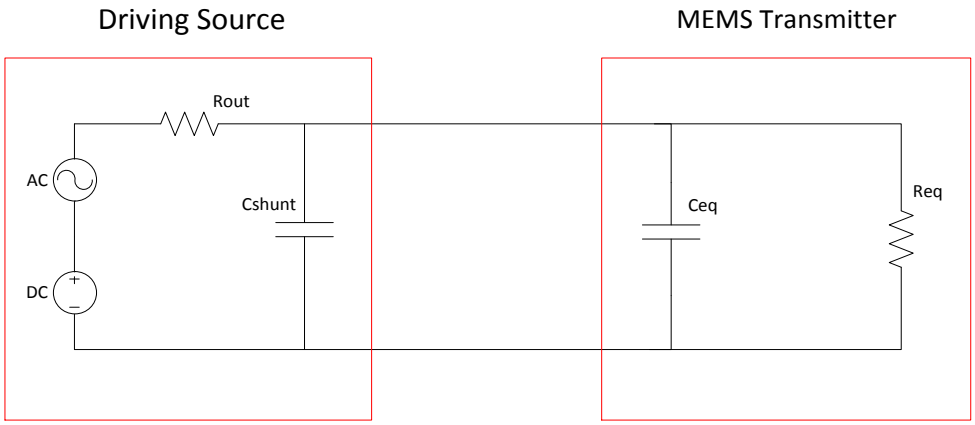

Figure 6-3: Coupled TFT/ MEMS Equivalent Circuit Model

The MEMS is shown on the right, and this is the model used for circuit simulations. The equivalent resistance and capacitance can be varied around critical "worst-case" values in order to design a robust circuit. In this simplified model, the driving source is represented as a simple RC circuit. In the circuit analysis, however, it will be treated as a switching amplifier.

A3: Electrical Equivalent Load Measurements of MEMS Devices

The figure below shows the equivalent resistance (Rp) and capacitance (Cp) if the load is assumed to function as a resistive element in parallel with a capacitive element. These data will form the basis for both simulation and experimental testing of the circuits designed for this project. In both simulation and experimental testing of these circuits, it is convenient to adopt a passive load. In this way the basic function of the electrical circuits can be verified. In order to confirm the dynamic performance will require further testing of the electronic circuits coupled with MEMS devices.

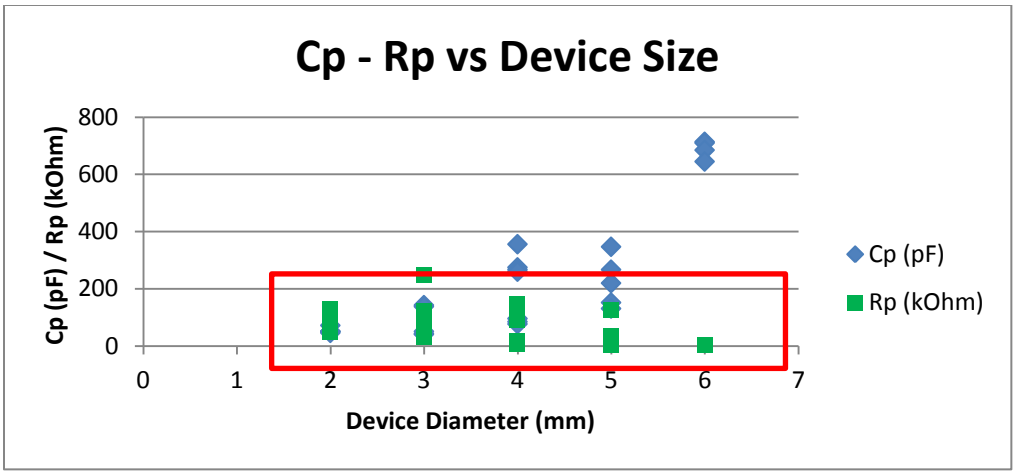

Figure 6-4: Equivalent Capacitance versus Device Diameter

This is a plot of Cp/Rp versus device diameter of typical MEMS devices. Not all of these devices are confirmed working acoustic devices, but the device structure and electronic performance is typical of working devices. Additionally, one may reasonably conclude that the high capacitance outliers are the result of the collapse of those device diaphragms. Thus it follows that the best working devices will operate within the range outlined in red. This is the range of equivalent resistance and capacitance used to simulate and test the circuit performance.

APPENDIX B
DATA COLLECTED JANUARY 2011 – OCTOBER 2012

APPENDIX B: OPTICAL AND ACOUSTIC TESTING

In order to understand the operation of the MEMS transducers in the context of this project, they must be considered for electrical and mechanical properties. Specifically, the mechanical response to electrical stimulus is extremely important [26][26]. The early MEMS devices were tested for their mechanical performance using external electrical stimulus in the form of a lab power supply and arbitrary waveform generator.

The first experiment measured the physical deflection of the devices in response to the electrical signal. The device under test was placed under an optical interferometer to measure the distance from the laser source to the device diaphragm. By operating the device under applied bias and alternating current stimulus, a deflection profile could be measured. The periodic distance between the laser source and the MEMS is plotted, and the difference between the minimum and maximum distance, the amplitude of the deflection profile, is the total periodic deflection of the MEMS diaphragm. If the MEMS diaphragm is treated as a cylindrical piston, this deflection profile can be used to calculate the total acoustic pressure generated [27][28].

To find the time independent pressure, use the following equation:

$$\boldsymbol{p(r,\theta) = j\omega\rho_0 a^2 v_n \frac{J_1(kasin\theta)}{kasin\theta}\frac{e^{jkr}}{r}}$$

Here, **p** is the pressure at a distance, **r**, from the piston at an angle, **θ**, from the normal vector.

To find the time dependent pressure, use the following equation:

$$p(r,\theta,t) = j\rho c\frac{Qk}{2\pi r}e^{j(\omega t-kr)}\frac{2J_1(kasin\theta)}{kasin\theta}$$

Here, **p** is the pressure at a distance, **r**, from the piston at an angle, **θ**, from the normal vector and at time, **t**, after some initial time.

It is possible to simplify this picture somewhat; the sound pressure output is related to the displacement of the diaphragm. Rather than immediately estimate the sound pressure at a given distance, it is possible to first find the displacement amplitude of a device for a given actuation voltage. The sound pressure at any distance is proportional to the amount that the diaphragm moves when actuated. The displacement equation can be written as:

$$D(V) = \frac{Cd_c}{2k_s(D_0 + D)^2}V^2$$

Here, **D** is the total displacement as a function of the applied voltage; **C** is the nominal capacitance; $\mathbf{d_c}$ is the constant of displacement, and $\mathbf{k_s}$ is the spring constant of the diaphragm.

Similarly, it is possible to relate the displacement to the frequency response of the devices. Again, the sound pressure at a given distance is proportional to the displacement. Therefore, if we relate the displacement for a given DC bias and AC actuation voltage with a variable frequency of actuation, this displacement frequency response should be proportional to the actual sound pressure frequency response of the device. The displacement versus frequency equation can be written as:

$$D(\omega) = \frac{Cd_c}{2k_s(D_0 + D)^2} V^2 * \frac{A}{\sigma\sqrt{2\pi}} e^{-\frac{1}{2c}\frac{(\omega-\omega_o)^2}{\sigma^2}}$$

$$D(f) = \frac{Cd_c}{2k_s(D_0 + D)^2} V^2 * \frac{A}{\sigma\sqrt{2\pi}} e^{-\frac{1}{2c}\frac{(2\pi(f-f_o))^2}{\sigma^2}}$$

Here, **D** is the total displacement as a function of the frequency; **C** is the nominal capacitance; $\mathbf{d_c}$ is the constant of displacement; $\mathbf{k_s}$ is the spring constant of the diaphragm; **c** is the speed of sound; $\boldsymbol{\omega_0}$ and $\mathbf{f_0}$ are the resonant angular frequency and resonant frequency respectively; **A** is the area constant of the normal distribution and σ is the variance of the normal distribution.

Optical Testing

The theoretical displacement versus applied voltage can be compared with the actual displacement measurements as shown below. The displacement of the diaphragm is measured using an optical interferometer while the devices is actuated using a DC voltage bias and AC voltage signal.

The results of the surface interferometer experiment are shown below:

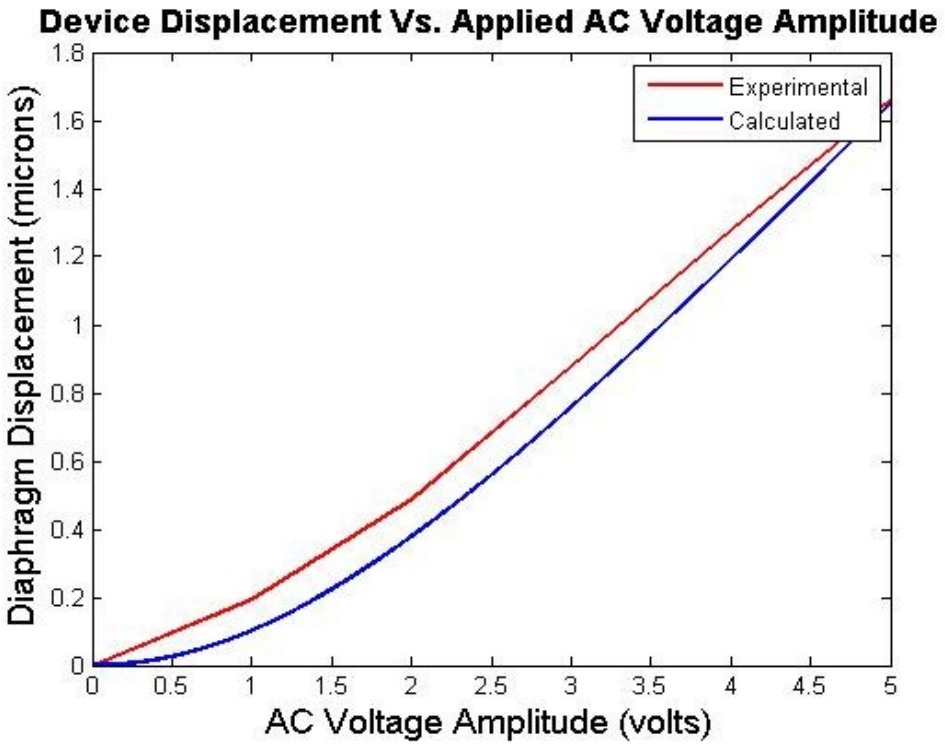

Figure 7-1: Diaphragm Displacement versus Applied AC Voltage

Diaphragm displacement for a typical MEMS electrostatic transducer for various applied AC voltage amplitudes. The DC bias is fixed at 10.25 V and the frequency is fixed at 5 kHz. The experimental result is compared with the theoretical calculation from the formula above.

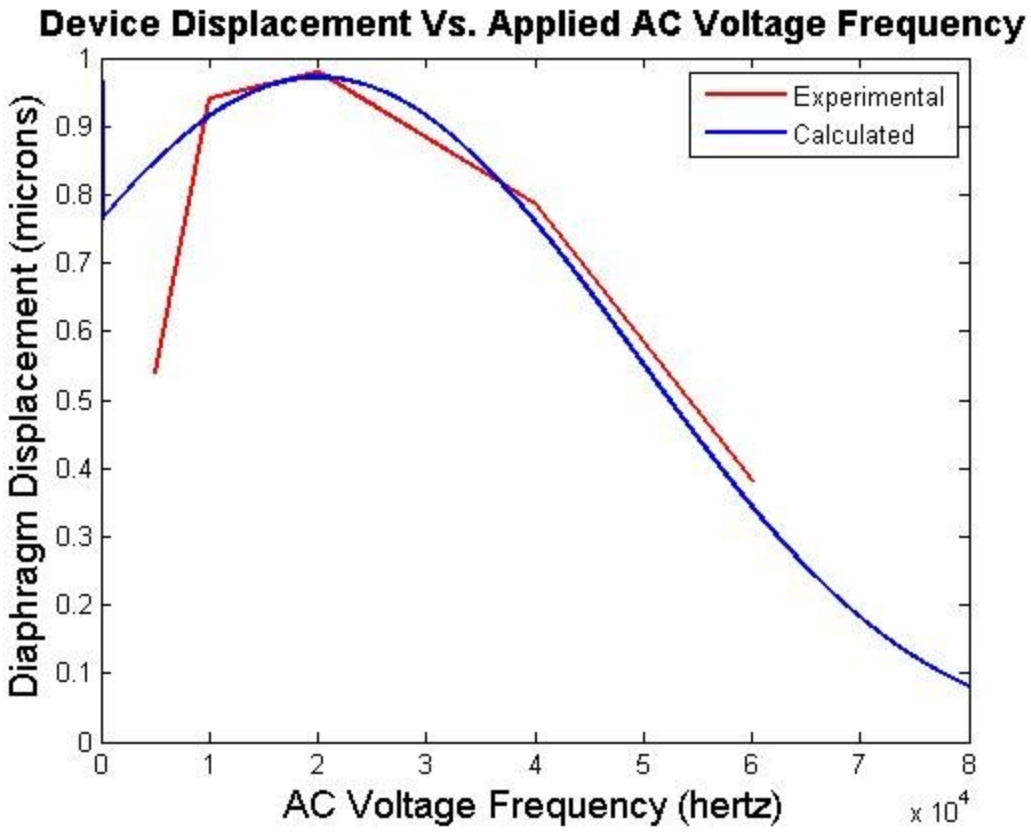

Figure 7-2: Diaphragm Displacement versus Applied AC Frequency

Diaphragm displacement for a typical MEMS electrostatic transducer for various applied AC voltage frequencies. The DC bias is fixed at 13.38 V and the AC amplitude is fixed at 5 V. The experimental result is compared with the theoretical calculation from the formula above.

Consider once again the model of the MEMS diaphragm as a vibrating acoustic piston. The equations for the sound pressure at a particular distance and angle were given earlier in the text. This model can be simplified by removing the angular dependence and simply taking the sound pressure level at a distance from the center of the diaphragm along a vector normal to the surface of the diaphragm.

The time independent pressure at a distance **r**:

$$\boldsymbol{p(r) = j\omega\rho_0 a^2 v_n \frac{e^{jkr}}{r}}$$

To find the time dependent pressure, use the following equation:

$$\boldsymbol{p(r,t) = j\rho c \frac{Qk}{\pi r} e^{j(\omega t - kr)}}$$

The next goal is to relate the displacement of the diaphragm with the sound pressure level. The amplitude of the periodic displacement can be related with the frequency of oscillation to find the average velocity of the diaphragm. The average velocity, $\boldsymbol{v(f,A) = 4fD}$, where **f** is the frequency of oscillation and D is the amplitude of the diaphragm displacement. The relationship between displacement and applied voltage has already been worked out, thus the relationship between projected sound pressure and applied voltage can be derived.

Acoustic Testing

In order to measure the acoustic performance of the MEMS devices, the devices were connected in the lab with a DC voltage source and digital waveform generator in series to provide a DC bias and AC driving signal. The DC bias was tuned to give the maximum sound output while the AC amplitude used was constant at 10 $V_{P\text{-}P}$. A commercial microphone was used to detect the acoustic signal. This signal was amplified and measured using a spectrum analyzer. The sound pressure level (SPL) was measured using a commercial SPL meter. A simple calibration was used to map the power spectral density (dB_M) measured from the microphone and spectral analyzer to the corresponding sound pressure

level (dB_{SPL}). This allows the SPL to be determined from the more accurate measurements of the microphone and spectral analyzer.

The results of the acoustic testing are compared with the theoretical calculations. The measurements were taken for sound pressure level versus distance. The devices were tested in a full array of acoustic transmitters, and individually. Additionally, there were devices fabricated on silicon and poly ethylene naphthalate (PEN); results are shown for both.

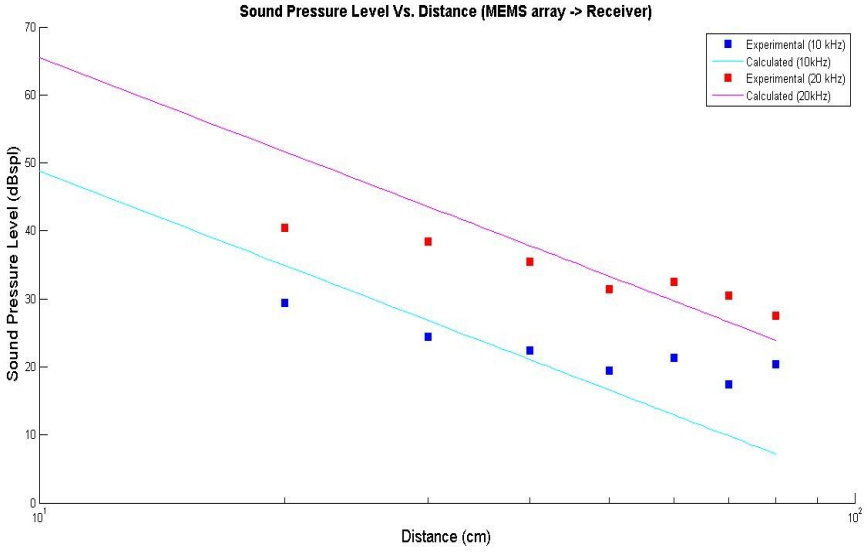

Figure 7-3: SPL versus Distance (MEMS Array)

This shows the acoustic sound pressure level measured at increasing distance from the array of MEMS transducers. The theoretical result is shown for comparison.

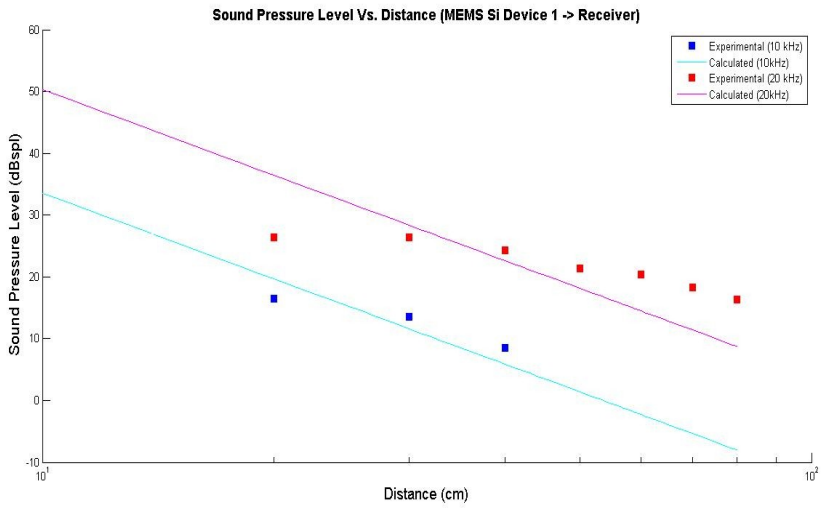

Figure 7-4: SPL versus Distance (MEMS on Silicon)

This shows the acoustic sound pressure level measured at increasing distance from single silicon based MEMS transducer. The theoretical result is shown for comparison.

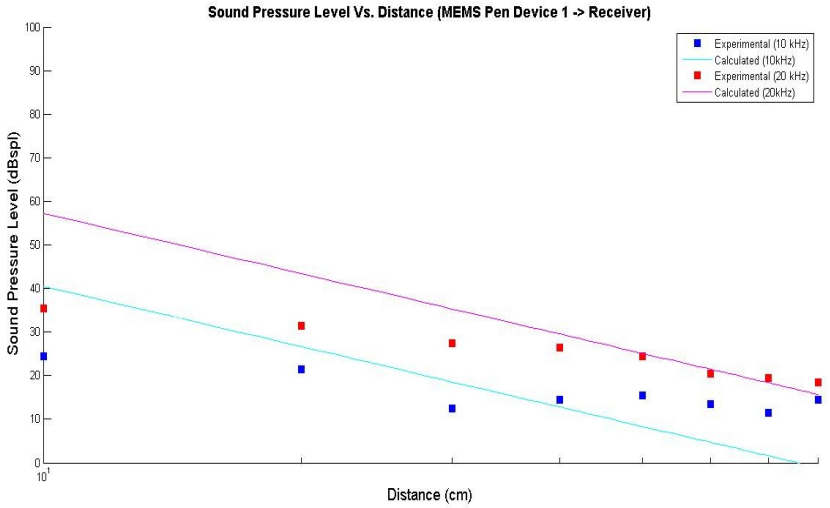

Figure 7-5: SPL versus Distance (MEMS on PEN1)

This shows the acoustic sound pressure level measured at increasing distance from single PEN based MEMS transducer. The theoretical result is shown for comparison.

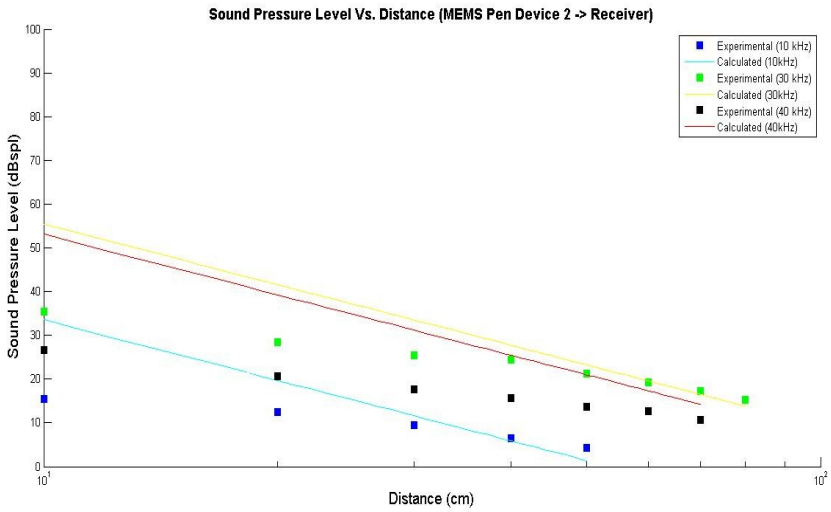

Figure 7-6: SPL versus Distance (MEMS on PEN2)

This shows the acoustic sound pressure level measured at increasing distance from single PEN based MEMS transducer. The theoretical result is shown for comparison.

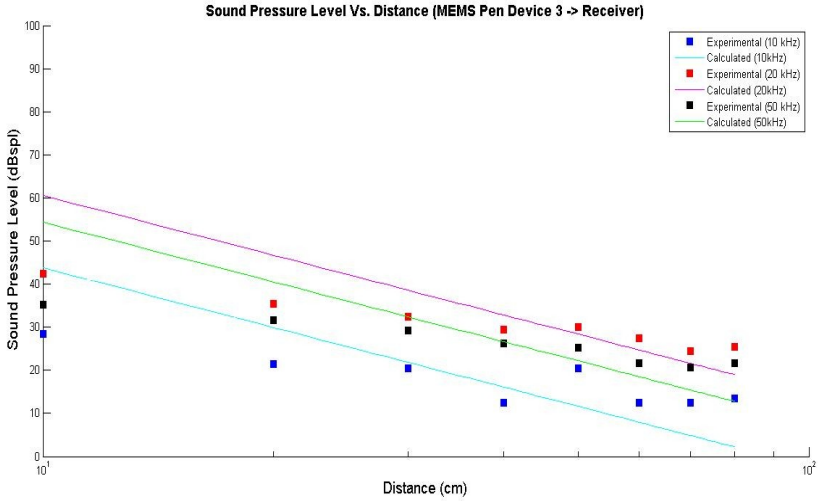

Figure 7-7: SPL versus Distance (MEMS on PEN3)

This shows the acoustic sound pressure level measured at increasing distance from single PEN based MEMS transducer. The theoretical result is shown for comparison.

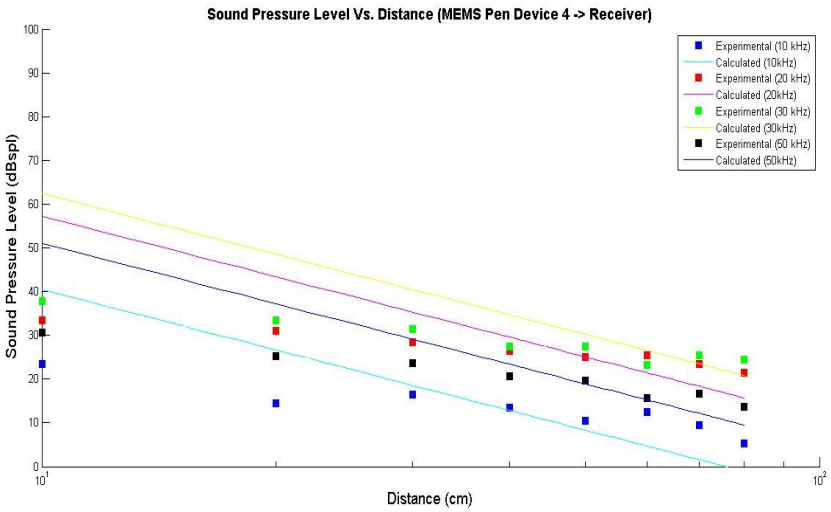

Figure 7-8: SPL versus Distance (MEMS on PEN4)

This shows the acoustic sound pressure level measured at increasing distance from single PEN based MEMS transducer. The theoretical result is shown for comparison.

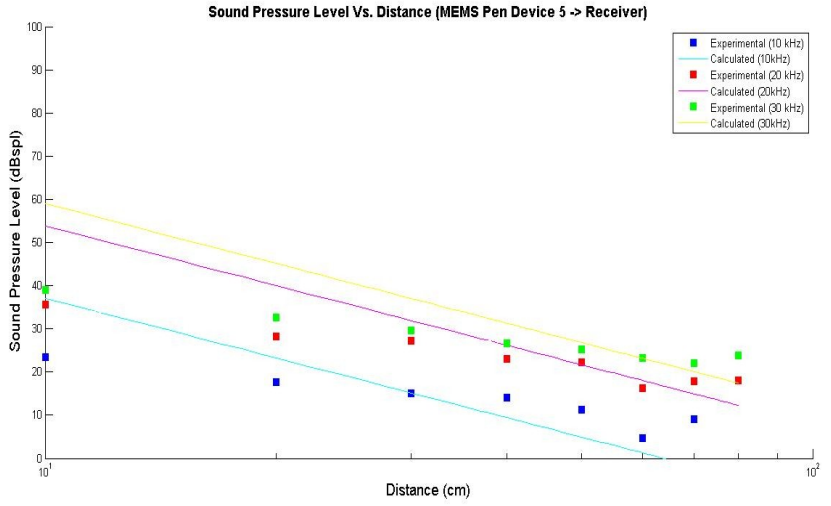

Figure 7-9: SPL versus Distance (MEMS on PEN5)

This shows the acoustic sound pressure level measured at increasing distance from single PEN based MEMS transducer. The theoretical result is shown for comparison.

APPENDIX C
DATA COLLECTED JANUARY 2011 – OCTOBER 2012

APPENDIX C: MEMS TEST AND MEASUREMENT PROCEDURES

Optical Testing

Secure devices on a testing strip. Bond the device contacts to the soldering pads. Solder copper wire to the soldering pads.

Mount the testing strip on the micro-manipulator (translations stage) and connect the circuit as shown in figure 8-1:

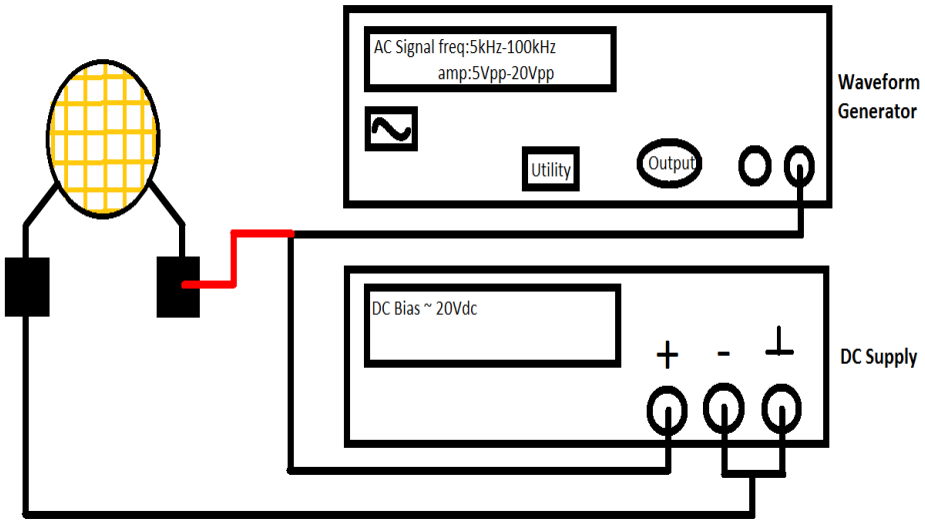

Figure 9-1: MEMS Optical Test Circuit

Test set up used to drive the MEMS transducers. Use a DC supply for bias and a waveform generator (WFG) for AC signal.

Aim the optical interferometer at the surface of the MEMS DUT

Connect the Optra as shown in figure 8-2:

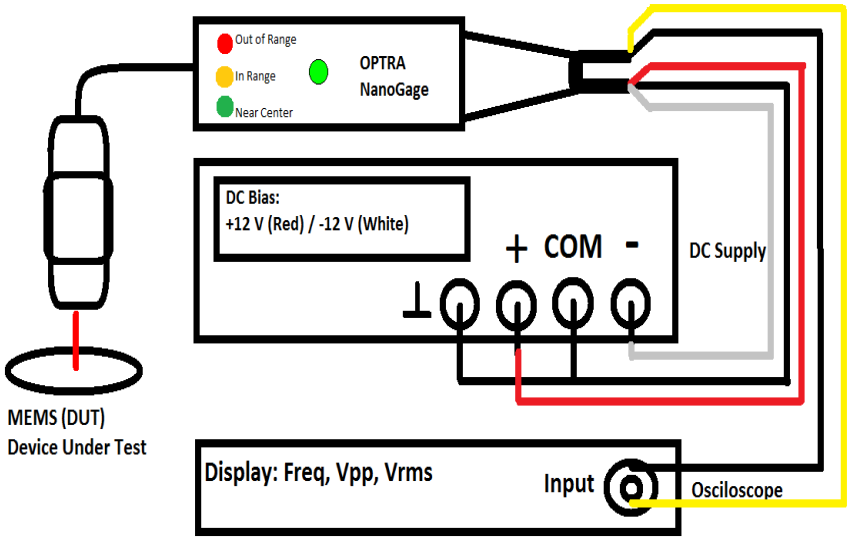

Figure 9-2: Optra Optical Test Circuit

Test set up used to power the optical interferometer (Optra). Use a DC supply for bias and an oscilloscope to measure the waveform.

Focus the optical beam by adjusting the height (z-axis) of the translational stage. (The x and y axis controls may need to be adjusted if the optical beam will not come into focus.)

Adjust the DC bias to 20 V_{DC}.

Set the WFG to output a sine wave.

Select Utility > Output Setup > High Z.

Adjust the output frequency to 5 kHz (10kHz, 20kHz, 50kHz, 100kHz)

Adjust the output amplitude to 5 V_{P-P} (10V_{P-P}, 20 V_{P-P})

Observe the output signal on the oscilloscope. The peak-to-peak voltage will correspond to peak-to-peak displacement of the MEMS diaphragm. It is important to record the outcome of each measurement, so use a scope that allows

saving to external memory. Because the output is a voltage corresponding to a vertical displacement, the test set-up may need to be routinely calibrated. As of Nov. 9 2010 the correlation is:

Range	Correlation
Near Field (optics too close to DUT)	4.3 mV/um
Near Center (green light)	2.4 mV/um
Far Field (optics too far from DUT)	5.4 mV/um

Testing Tip:

A DC bias of 20 V_{DC} is not always the ideal bias point. There are times when slightly lower bias will improve performance. This is likely do to damping effects, or a limited range of motion when the diaphragm air gap becomes too small. Try tuning the bias:

Observe the output waveform from the optical interferometer.
Slowly adjust the DC bias of the MEMS device, taking careful note of the output swing.

When the output swing is at the maximum attainable range, your DC bias has been tuned correctly. This should allow for optimum performance.

Acoustic Testing

Secure devices on a testing strip.

Bond the device contacts to the soldering pads.

Solder copper wire to the soldering pads.

Mount the testing strip on the rotational aperture (device side rail carrier) and connect the circuit as shown in figure 8-3:

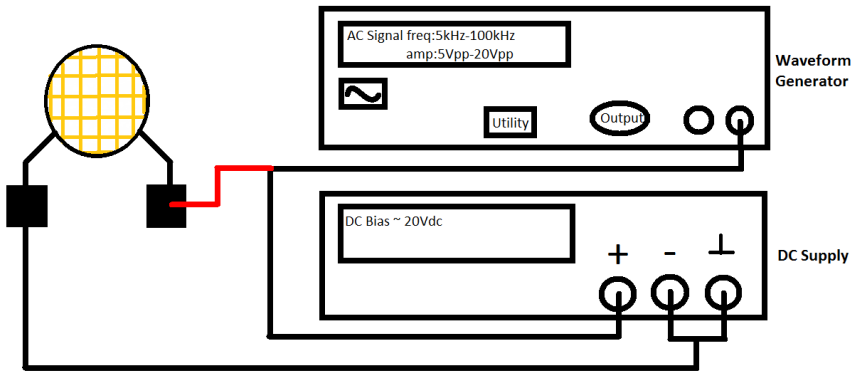

Figure 9-3: MEMS Acoustic Test Circuit

Test set up used to drive the MEMS transducers. Use a DC supply for bias and a waveform generator (WFG) for AC signal.

Aim the MEMS DUT towards the microphone.

Connect the microphone as shown in figure 8-4:

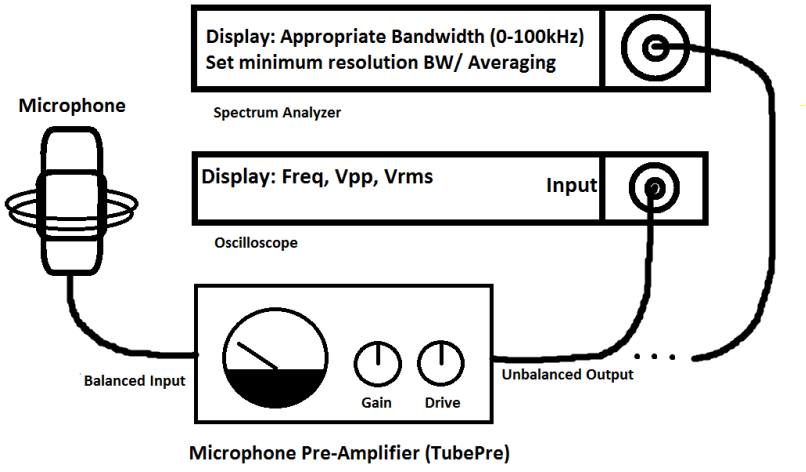

Figure 9-4: Acoustic Measurement Test Circuit

Test set up used to power the condenser microphone. Use the microphone amplifier to supply phantom power to the microphone and an oscilloscope to measure the waveform.

Focus the sound source by adjusting the height and lateral displacement (The x and y axis) of the translational stage. (The z axis is along the rail, used to control the distance of the measurement)

Adjust the rotational angle of the MEMS transmitter, first using the rough adjustment, then the fine tuning knob

Adjust the DC bias to 20 V_{DC}.

Set the WFG to output a sine wave.

Select Utility > Output Setup > High Z.

Adjust the output frequency to 5 kHz (10kHz, 20kHz, 50kHz, 100kHz) (5kHz, 10kHz, 15kHz, 20kHz, 25kHz, 30kHz, 35kHz, 40kHz for audio mic)

Adjust the output amplitude to 5 V_{P-P} (10 V_{P-P}, 20 V_{P-P})

Begin with a distance of 10 cm in order to facilitate accurate alignment. Repeat all of your measurements at each desired distance. The range should be increased in a uniform manner, choosing a linear scale for short distances and moving to a decade scale for longer distances.

(10cm, 15cm, 20cm, 25cm, 30cm, 40cm, 50cm, 75cm, 100cm, 250cm, 500cm, 1m, 1.5m, 2m, etc.)

Continue increasing the distance until the signal is lost entirely!

Observe the output signal on the oscilloscope. The RMS voltage will be used to determine sound pressure level. Use the calibration data to determine this correlation.

Observe the output signal on the spectrum analyzer. This will be a decibel scale output corresponding to the sound pressure level. Use the calibration data to determine this correlation.

Please record the following for each experiment:

Applied DC bias

Applied AC signal (including frequency)

Received signal (Vpp, Vrms, Frequency, SNR)

Spectrum data (Spectral Peak, SNR)

Because the output is a voltage corresponding to a SPL, the test set-up may need to be routinely calibrated. Calibration procedures are discussed below.

Calibration Procedure:

Configure the experimental setup as you would for normal testing.

Replace the MEMS device with a suitable sound source (speaker)

In addition to the microphone, place the SPL meter in the direct vicinity of the receiving end to monitor sound pressure level.

Connect the speaker to a WFG, keep in mind there is no need for DC bias

Apply whatever AC signal is required to achieve the appropriate voltage output (in the range of 10 mV up to 2-10 V). A wide range of receiver voltage is necessary to characterize the system.

Repeat this procedure for frequencies of 4-8kHz (the operating range of the SPL meter)

Plot the SPL versus receiver voltage (RMS) at various frequencies. These plots will help to develop a model which maps the microphone output to a corresponding sound pressure level. We will need this model in order to present our MEMS results in terms of sound pressure level.

Spectrum Analyzer Calibration

In the interest of reporting the results of acoustic measurements in terms of normalized sound pressure (SPL) it is necessary calibrate the spectrum analyzer. The goal of this calibration is to find the correlation between the electrical power (dBm) measured by the spectrum analyzer. This power measurement is NOT directly coupled from the devices themselves, it is measured from the output of an amplifier which is used to boost the signal strength of the microphone used for the measurement. Despite the additional coupling stages, the only significant loss mechanism to affect the measurements is the acoustical interface (in this case, air). The conclusion of this observation is that certain fundamental relationships will remain intact (ie. distance of transmission vs. sound pressure of the signal at the receiver). A simple calibration is required to interpret the measurements.

Note to reader:

This calibration is subject to error in predictable ways, however it may be difficult to correct for this error. For instance, in the example shown both the calibration and sample data were collected using an Audio Technica AT-2035

microphone. The microphone specifications report a noise floor of 20 dB SPL, but the calibration of sample data reports values of SPL less than 20 dB. How can this be explained?

1) The calibration suffers from one or more of the following
    a. False assumptions regarding the power transfer coefficient
    (Given the repetitive nature of the experiment and the consistency of the strength of correlation in the model this has been ruled out)
    b. Anomalous readings from the SPL meter
    (This could due in part to the frequency response of the SPL meter, or due to the fact that it does not distinguish frequencies one from another)
    c. The calibration must be performed in a frequency range which is inconsistent with that of the sample data (this is unfortunate, but has no apparent remedy)
2) The microphone specification does not discuss frequency referred noise
    a. The noise floor specification of the microphone must be valid throughout the range of performance in order to be valid (20 Hz – 20 kHz)
    b. In a typical environment (even a strictly controlled "sound proof" environment) the ambient noise is more powerful at low frequency
    c. A 20 dB noise floor at 20 Hz does NOT imply a 20 dB noise floor at 20 kHz and above

Calibration Requirements:

In order to complete the calibration experiment, a number of materials and equipment are required:

1) The spectrum analyzer to be used in future experiments
2) The microphone/amplifier to be used in future experiments
3) A speaker to be used for reference sound generation
4) A waveform generator to drive a signal to the speaker
5) A sound pressure level meter to record the reference SPL

Optionally, a rail system may be employed to aid in the alignment of the transmitter (speaker) and receiver (microphone)

Calibration Procedure:

Set Up

1) Align the microphone and test speaker at a distance greater than the limit for near field effects (~5 cm) The recommended distance is 10 cm
2) Align the SPL meter such that the sensing element is the same distance from the speaker and at approximately the same altitude as the microphone
3) Use the waveform generator to drive the speaker; this allows for variable frequency and actuation voltage in order to perform the calibration

Performance

1) Set the frequency range of your spectrum analyzer in the range of calibration (this is typically limited by the SPL meter chosen)
2) Set both the waveform generator frequency and the measurement frequency of the spectrum analyzer at the frequency f_0
3) Set the WFG to output a sine wave, beginning with the minimum amplitude available
4) Monitor the SPL and the spectral power of the signal, record both
5) Repeat steps 2-4 for an appropriate range of frequency and sound pressure output

Frequency: Vary frequency in the range of interests with 4-8 discrete frequencies

Power: Record measurements for outputs in the entire range of the WFG in intervals of 1dBm

Following this procedure will calibrate for SPL values in the range of interest. Typically extrapolation is required due to the relatively high noise floor of most SPL meters; additionally the inability to distinguish frequency makes SPL meters susceptible to the full spectrum of noise.

Calibration Result:

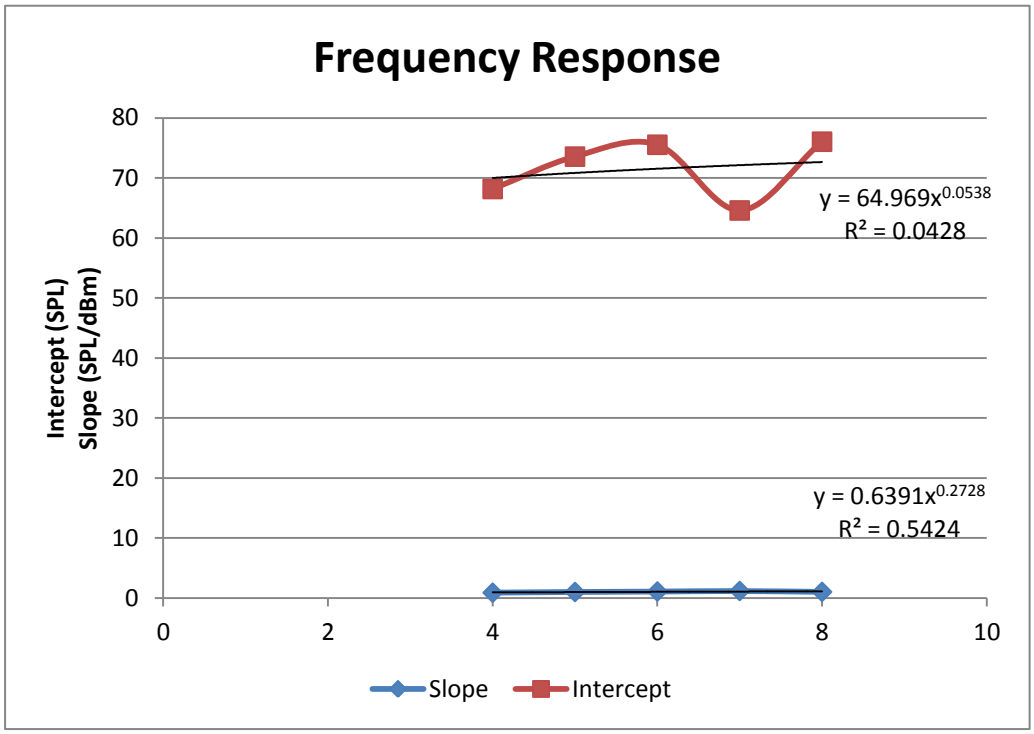

Figure 9-5: Spectrum Analyzer Calibration

This plot shows the slope and intercept found when plotting the linear correlation between the measured sound pressure level from the SPL meter and the measured power spectral density from the spectrum analyzer.

Discussion of Results:

By analyzing the results, we can derive an equation to relate sound pressure level and spectral power. This allows for results measured using the spectrum analyzer to be presented in terms of the sound pressure level:

$$SPL\ (dB) = K(f) * P(dBm) + C(f)$$

Where K is the power transfer coefficient and C is the nominal SPL at P = 0 dBm.

Initially, the model used included the apparent frequency dependence of both the power transfer coefficient and the nominal sound pressure. The results were not consistent with reason, as subsequent experiments returned measurements of negative relative sound pressure level. A normalized sound pressure of SPL < 0 dB is a sound that is theoretically below the threshold of human hearing. Additionally the sound threshold of most microphones is much higher around 10-20 dB.

Removing the frequency dependence of the power transfer coefficient allowed for a model which still reflected the moderate frequency dependence of the nominal sound pressure level. This result allowed for much more realistic estimations of the sound pressure when measuring with a typical microphone.

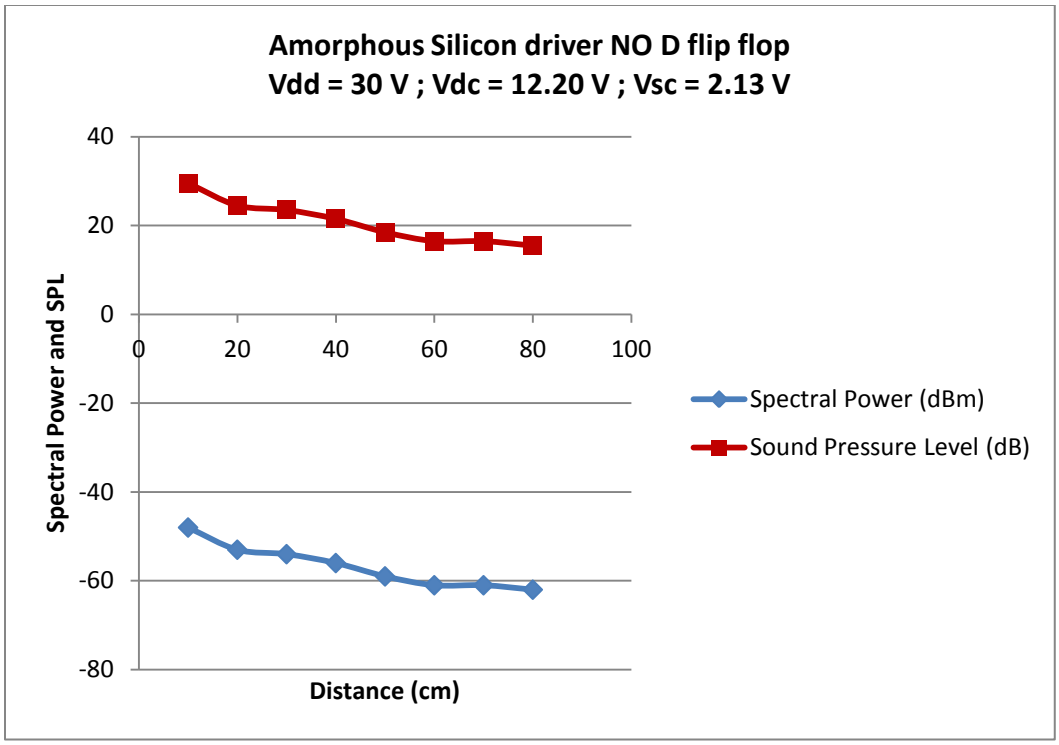

Figure 9-6: Calibrated Spectrum Analyzer Data

An example showing the calibration applied to measured data.